JOURNAL OF PETROLOGY

Journal of Petrology, 2016, Vol. 57, No. 11&12, 2195–2220
doi: 10.1093/petrology/egw074
Original Article

OXFORD

A Reactive Porous Flow Control on Mid-ocean Ridge Magmatic Evolution

C. Johan Lissenberg* and Christopher J. MacLeod

School of Earth and Ocean Sciences, Cardiff University, Park Place, Cardiff CF10 3AT, UK

*Corresponding author. Telephone: +44 2920 874 327. Fax +44 2920 874 32. E-mail: lissenbergcj@cardiff.ac.uk

Received December 24, 2015; Accepted December 24, 2016

ABSTRACT

Mid-ocean ridge basalts (MORB) provide fundamental information about the composition and melting processes in the Earth's upper mantle. To use MORB to further our understanding of the mantle, is imperative that their crustal evolution is well understood and can thus be accounted for when estimating primary melt compositions. Here, we present the evidence for the occurrence of reactive porous flow, whereby migrating melts react with a crystal mush in mid-ocean ridge magma chambers. This evidence comprises both the textures and mineral major and trace element geochemistry of rocks recovered from the lower oceanic crust, and occurs on a range of scales. Reaction textures include dissolution fronts in minerals, ragged grain boundaries between different phases and clinopyroxene–brown amphibole symplectites. However, an important finding is that reaction, even when pervasive, can equally leave no textural evidence. Geochemically, reactive porous flow leads to shifts in mineral modes (e.g. the net replacement of olivine by clinopyroxene) and compositions (e.g. clinopyroxene Mg–Ti–Cr relationships) away from those predicted by fractional crystallization. Furthermore, clinopyroxene trace elements record a progressive core–rim over-enrichment (relative to fractional crystallization) of more-to-less incompatible elements as a result of reactive porous flow. The fact that this over-enrichment occurs over a distance of up to 8 mm, and that clinopyroxenes showing this signature preserve zoning in Fe–Mg, rules out a diffusion control on trace element distributions. Instead, it can be explained by crystal–melt reactions in a crystal mush. The data indicate that reactive flow occurs not only on a grain scale, but also on a sample scale, where it can transform one rock type into another [e.g. troctolite to olivine gabbro, olivine gabbro to (oxide) gabbro], and extends to the scale of the entire lower oceanic crust. Melts undergoing these reactive processes change in composition, which can explain both the major element and trace element arrays of MORB compositions. In particular, reactive porous flow can account for the MORB MgO–CaO–Al_2O_3 relationships that have previously been interpreted as a result of high-pressure (up to ~8 kbar) crystal fractionation, and for over-enrichment in incompatible elements when compared with the effects of fractional crystallization. The finding of a significant role for reactive porous flow in mid-ocean ridge magma chambers fits very well with the geophysical evidence that these magma chambers are dominated by crystal mush even at the fastest spreading rates, and with model predictions of the behaviour of crystal mushes. Together, these observations indicate that reactive porous flow is a common, if not ubiquitous, process inherent to mushy magma chambers, and that it has a significant control on mid-ocean ridge magmatic evolution.

Key words: gabbro; lower oceanic crust; mid-ocean ridge; mid-ocean ridge basalt; reactive porous flow

INTRODUCTION

Mid-ocean ridge basalt (MORB) is the most abundant volcanic rock on Earth. Critically, MORB magmas provide the geochemist with a window into the upper mantle: because they are formed directly by decompression melting of the mantle and do not traverse thick, older crust, their compositions are considered to directly reflect the composition and melting processes of their mantle source (e.g. Klein & Langmuir, 1987). This approach, however, requires that the crustal evolution of MORB can be corrected for. This is conventionally done by assuming that the crustal evolution is predominantly controlled by fractional crystallization. Given that fractional crystallization of MORB is well constrained (e.g. Grove *et al.*, 1992), this assumption has allowed MORB compositions to be parameterized in terms of degree and depth of melting, as well as source compositions (Langmuir *et al.*, 1992). However, a substantial range of data collected over the last decades has provided evidence indicating that the crustal evolution of MORB is complex, involving more than fractional crystallization alone. This evidence comes from both MORB itself as well as mid-ocean ridge plutonic rocks. From a MORB perspective, open-system processing has long been established to play a role [e.g. Dungan & Rhodes, 1978; Rhodes *et al.*, 1979; see Shorttle (2015) for a recent perspective]. Furthermore, the observation initially made in the 1970s that mid-ocean ridge basalts are enriched more strongly in incompatible trace elements with decreasing MgO or Mg# than predicted by fractional crystallization (Bryan & Moore, 1977; White & Bryan, 1977; Dungan & Rhodes, 1978) has been highlighted again in recent years (O'Neill & Jenner, 2012; Lissenberg *et al.*, 2013). Similar observations have been made in Iceland (Eason & Sinton, 2009). This signature has been variably interpreted as reflecting replenishment cycles (O'Neill & Jenner, 2012), *in situ* crystallization (Coogan & O'Hara, 2015) or melt–rock interaction (Eason & Sinton, 2009; Lissenberg *et al.*, 2013) in oceanic magma chambers. Whichever model is correct, it demonstrates that crustal processing may exert a strong signature on the erupted lavas. This is further highlighted by the occurrence of ultra-depleted, high-Al melt inclusions in MORB phenocrysts, which result from the interaction of MORB with lower crustal lithologies (Danyushevsky *et al.*, 2003; Kamenetsky & Gurenko, 2007; Laubier *et al.*, 2012).

Plutonic rocks recovered from the lower oceanic crust also record complex histories. Complex zoning patterns, reaction textures, as well as mineral compositions and modes that do not conform to conventional phase equilibria, all indicate that fractional crystallization is not the only process controlling their formation (Meyer *et al.*, 1989; Coogan *et al.*, 2000; Dick *et al.*, 2002; Ridley *et al.*, 2006; Gao *et al.*, 2007; Lissenberg *et al.*, 2013). Similar observations have been made for ophiolitic magma chambers (Bédard, 1991; Bédard *et al.*, 2000; Sanfilippo *et al.*, 2015*b*).

In summary, the available data indicate that crustal processing of MORB is complex. Hence, if we want to understand the mantle, it is imperative that we first understand the overprint imparted by the crust. As part of this effort, in this contribution we present the textural and geochemical evidence for reactive porous flow (RPF) in mid-ocean ridge magma chambers, and discuss its link to the observed array of MORB compositions. We conclude that reactive porous flow is a very common—if not ubiquitous—process in oceanic magma chambers, and that it plays a significant role in modifying MORB.

THE RECORD OF REACTIVE POROUS FLOW IN PLUTONIC ROCKS

In this section, we review the evidence for reactive porous flow in plutonic rocks from the grain scale to the lower crustal scale. We focus predominantly on plutonic rocks from three locations in the ocean basins: Hess Deep, the Kane Megamullion and Ocean Drilling Program (ODP) Hole 735B. Hess Deep exposes a lower crustal section through 1·2 Ma lower crust formed at the East Pacific Rise (Francheteau *et al.*, 1990; Rioux *et al.*, 2012) and represents fast-spreading lower crust (spreading rate $\sim$130 mm a^{-1}). An extensive sample collection (93 gabbroic rocks) was recovered during expedition JC-21, ranging from primitive gabbroic rocks intercalated with peridotites at the base to evolved oxide gabbros and gabbronorites near the base of the sheeted dyke complex at the top (Lissenberg *et al.*, 2013). As such, the Hess Deep JC-21 samples are the only suite representing a more or less complete stratigraphic section of the lower oceanic crust anywhere in the oceans. The Kane Megamullion (23°N, Mid-Atlantic Ridge) exposes the plutonic foundation of a 50 km long, second-order, slow-spreading (23 mm a^{-1}) ridge segment, which was extensively mapped and sampled during expedition KN180-2 (Dick *et al.*, 2008). Plutonic rocks formed in a series of magmatic centres surrounded by weakly magmatic peridotite-dominated areas (Dick *et al.*, 2008; Xu *et al.*, 2009), and span the entire compositional spectrum of oceanic plutonic rocks, from olivine-rich troctolites to oxide gabbros (Dick *et al.*, 2008). ODP Hole 735B drilled 1508 m into gabbroic rocks unroofed at the Atlantis Bank core complex on the Southwest Indian Ridge, recovering a plutonic section dominated by series of generally coarse-grained olivine gabbros cross-cut by more evolved rocks (gabbronorites, oxide gabbros) and subordinate troctolite (Dick *et al.*, 2000). It formed at a spreading rate of 15·7 mm a^{-1} (Baines *et al.*, 2007), which is transitional between slow and ultraslow (Dick *et al.*, 2003). With >20 000 electron microprobe analyses available (Dick *et al.*, 2002), it is the best-documented section of oceanic lower crust. The combined sample sets from Hess Deep, the Kane Megamullion and ODP Hole 735B cover the three main ocean basins, and encompass nearly the full spreading rate spectrum; hence, they provide a relatively rigorous

picture of the nature of the lower oceanic crust. Although ophiolitic plutonic sections also contain abundant evidence for melt–rock reaction (Bédard, 1991; Bédard *et al.*, 2000; Sanfilippo *et al.*, 2015*b*), they commonly contain rocks of different parentage (e.g. MORB-like, fore-arc basalt, island-arc tholeiite, boninite). In this setting, melt–rock reaction may be enhanced by the increased differences in major element compositions and water contents between different magma batches and their crystallization products; hence, this may not directly inform inferences about mid-ocean ridge magmatic evolution. We have therefore excluded from this study observations made in ophiolites, with one exception (trace element distributions in the Oman ophiolite lower crust).

RPF at the grain scale

Textures

Reactions between melts and crystals commonly leave behind textural evidence. Arguably the most common is the presence of dissolution fronts in plagioclase (Fig. 1a). Widely described, these comprise irregular contacts between zones of different anorthite content. The difference in anorthite contents of the different zones indicates that different parental melts were involved in crystallization of the crystal, with the morphology of the contact providing evidence of a reactive origin. Dissolution fronts can be distinguished from other forms of anorthite zoning (e.g. oscillatory and continuous zoning), which do not require reaction, by the contact between the different zones being irregular and discordant to the crystallographic axes (Fig. 1a). This commonly results in embayed habits. Dissolution fronts in plagioclase do not in themselves require RPF; they are common in phenocrysts in MORB where they result from the incorporation of earlier-formed crystals in new magma batches (e.g. Dungan & Rhodes, 1978). In this scenario, disequilibrium between the crystals and the carrier melt may result in dissolution. Evidence that at least some plagioclase dissolution fronts result from RPF comes from plutonic rocks in which the dissolution process was 'frozen in'. An example of this was presented by Lissenberg & Dick (2008), who described centimetre-wide channels of coarse-grained, poikilitic

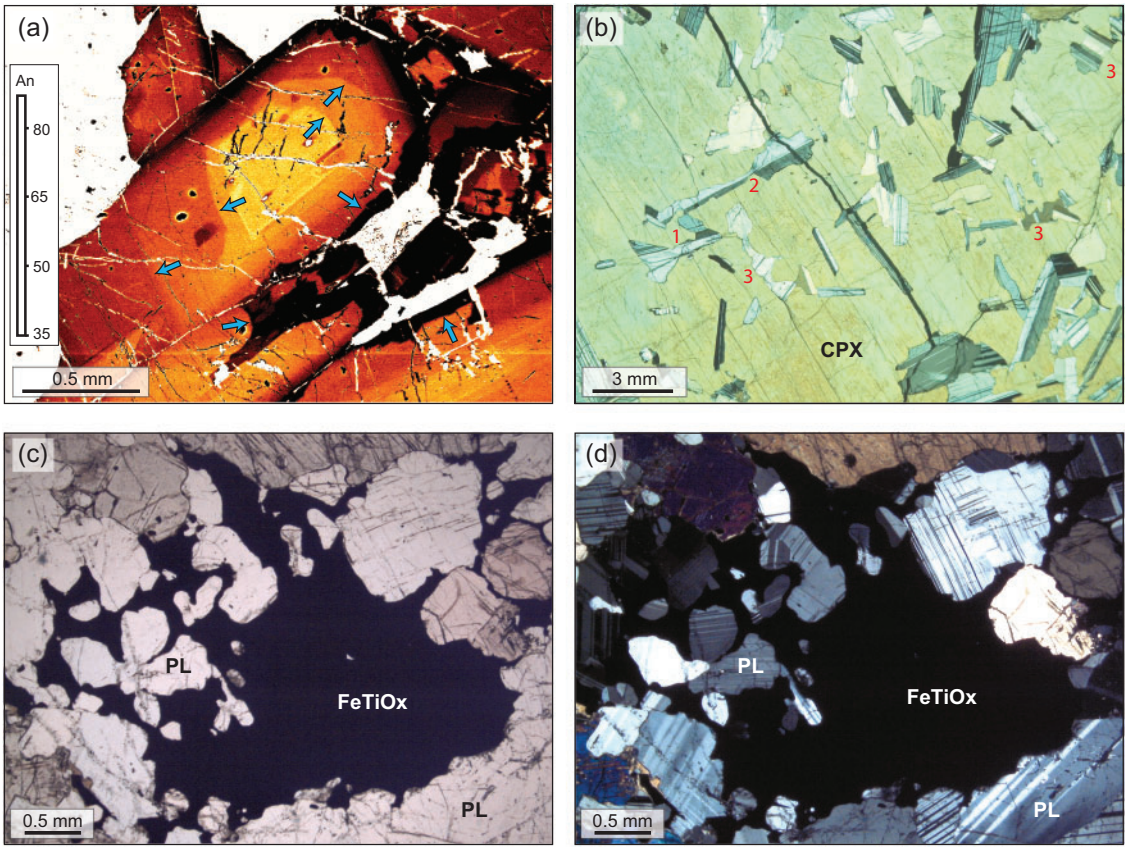

Fig. 1. Plagioclase textures associated with RPF. (a) Anorthite (An) map obtained from a BSE image and scaled using electron microprobe data from Lissenberg *et al.* (2013), showing dissolution fronts (blue arrows) in plagioclase in gabbro from Hess Deep (Pacific Ocean). (b) Plagioclase dissolution textures in a clinopyroxene oikocryst from a Kane Megamullion gabbro (Lissenberg & Dick, 2008). Dissolution results in irregular, embayed crystals with grain boundaries that are discordant to the crystallographic axes (highlighted by 1), and locally dissolution has proceeded the extent that parts of originally millimetre-sized grains become very thin (~100 μm; location 2). Some grains have become elongate in the direction of the *a*- or *b*-axis as a result of dissolution (sub)parallel to the *c*-axis (3). (c, d) Dissolution of plagioclase by Fe–Ti oxide-saturated melt preserved as highly corroded, embayed plagioclase relics in Fe–Ti oxide (oxide gabbro, ODP Hole 735B, Southwest Indian Ridge). CPX, clinopyroxene; FeTiOx, Fe–Ti oxide; PL, plagioclase.

gabbro in a medium-grained troctolite host rock from the Kane Megamullion (23°N, Mid-Atlantic Ridge). These channels formed by the percolation of clinopyroxene-saturated melts through the troctolite, which led to the melt reacting with olivine, plagioclase and Cr-spinel in the troctolite to yield clinopyroxene and lower-anorthite plagioclase in the reaction [modified from Lissenberg & Dick (2008) to incorporate the dissolution of spinel]:

$$\text{olivine} + \text{plagioclase 1} + \text{Cr} - \text{spinel} + \text{melt 1} = \text{clinopyroxene} + \text{plagioclase 2} + \text{melt 2}. \quad (1)$$

The dissolution of the plagioclase is captured by the plagioclase chadacrysts enclosed in the clinopyroxene: plagioclase chadacrysts have highly irregular shapes, with curved grain boundaries discordant to the crystallographic axes (Fig. 1b). Competition during co-crystallization of plagioclase and clinopyroxene can be ruled out as a cause of these textures, because plagioclase ($An_{65–67}$) is not in equilibrium with clinopyroxene (Mg 86–87) (Lissenberg & Dick, 2008). In places, dissolution has proceeded to the extent that only very thin (100 μm) plagioclase relics remain of what otherwise were millimetre-sized crystals. Remarkably, some plagioclase crystals were dissolved (sub)parallel to their albite twins (i.e. *a*- to *c*-axis, depending on crystal orientation in the thin section), resulting in grains that are now elongated perpendicular to their twins (i.e. along their shorter *a*- or *b*-axes; Fig. 1b); hence, plagioclase morphology can become disconnected from its usual crystal habit. Similar textures to the ones described here have been found in other oceanic gabbro studies. Blackman *et al.* (2006) described rounded and resorbed plagioclase chadacrysts in pyroxene oikocrysts from Intergrated Ocean Drilling Program (IODP) Hole U1309D (30°N, Mid-Atlantic Ridge), and corroded plagioclase inclusions in clinopyroxene oikocrysts occur in gabbros recovered from IODP Hole 1256D in the equatorial Pacific Ocean (Teagle *et al.*, 2006). Where the reactive melt is more evolved and saturated in Fe–Ti oxides, a distinct texture of irregularly shaped, resorbed plagioclase 'islands' in Fe–Ti oxides may develop (Fig. 1c and d). The resorbed plagioclase shares many characteristics with its clinopyroxene-hosted counterparts described above: curved grain boundaries discordant to the crystallographic axes, grains elongated along *a*- to *b*-axes, and the presence of narrow relicts of former grains (Fig. 1c and d).

Clinopyroxene also preserves textural evidence for reaction with melts. In gabbroic rocks from ODP Hole 735B (Southwest Indian Ridge), complexly intergrown, ragged clinopyroxene–clinopyroxene grain boundaries are commonly present (Fig. 2a and b). Furthermore, cumulus clinopyroxene crystals commonly contain zones with small (~10–100 μm) blebs of brown amphibole (Fig. 2c and d). These zones can occur throughout the clinopyroxene grains, including areas apparently far from grain boundaries. The example shown in Fig. 2c and d occurs within a large (~2 cm) cumulus clinopyroxene grain. Their brown color, high Ti contents and their association with other magmatic phases such as Fe–Ti oxides, indicate a magmatic, not hydrothermal origin for the amphibole (e.g. Coogan *et al.*, 2001). The brown amphibole blebs are associated with recrystallized clinopyroxene, which indicates that the following reaction was responsible for their formation:

$$\text{clinopyroxene 1} + \text{melt 1} = \text{clinopyroxene 2} + \text{amphibole} + \text{melt 2}. \quad (2)$$

The same reaction is marked by clinopyroxene–amphibole symplectites that are common in both 735B gabbros and high-level gabbros from Hess Deep. These symplectites form at the expense of original cumulus clinopyroxene, invading the pre-existing clinopyroxene from their grain boundaries (Fig. 2e–h); this is a form of so-called hydration crystallization reactions (Beard *et al.*, 2004).

It is important to note, however, that RPF does not necessarily leave any textural evidence: it may be cryptic, with extensive modifications in mineral chemistry in texturally pristine cumulates. A case in point is the deepest and one of the most primitive olivine gabbros recovered from Hess Deep (Fig. 3). This olivine gabbro shows a classic equilibrated texture of cumulus olivine, plagioclase and clinopyroxene (Fig. 3a). Grain boundaries are sharp and commonly straight, and there is no textural evidence for the presence of a trapped, evolved melt (e.g. no interstitial brown amphibole and Fe–Ti oxides) or any reactions in the form of dissolution fronts, symplectites or complex plagioclase zoning. A Ti–Cr element map (Fig. 3b; see Supplementary Data for method), however, reveals that all clinopyroxene crystals are zoned, with Cr-rich cores giving way to Ti-rich rims. In principle, the presence of Cr–Ti zoning is in itself consistent with fractional crystallization. However, as we will discuss below (in the section on mineral trace elements), this kind of Cr–Ti zoning is an excellent indicator of core–rim incompatible trace element enrichment owing to RPF. Hence, even in rocks lacking any textural evidence for the process, RPF may be pervasive.

Mineral major and minor elements

Because the compositions of mineral phases reflect the evolution of the melt from which they crystallize, they form a solid line of descent to complement the melt's liquid line of descent. Such a solid line of descent is readily observable in global compilations of mineral compositions (Coogan, 2014), and, in clinopyroxene, is characterized by an exponential decrease in Cr_2O_3 and increase in TiO_2 with decreasing Mg#. However, there are some significant deviations from these overall trends, leading to Mg–Ti–Cr relationships that appear contradictory to well-established phase equilibria. One of these is the occurrence of clinopyroxene with unusually high Mg#. At lower oceanic crustal pressures

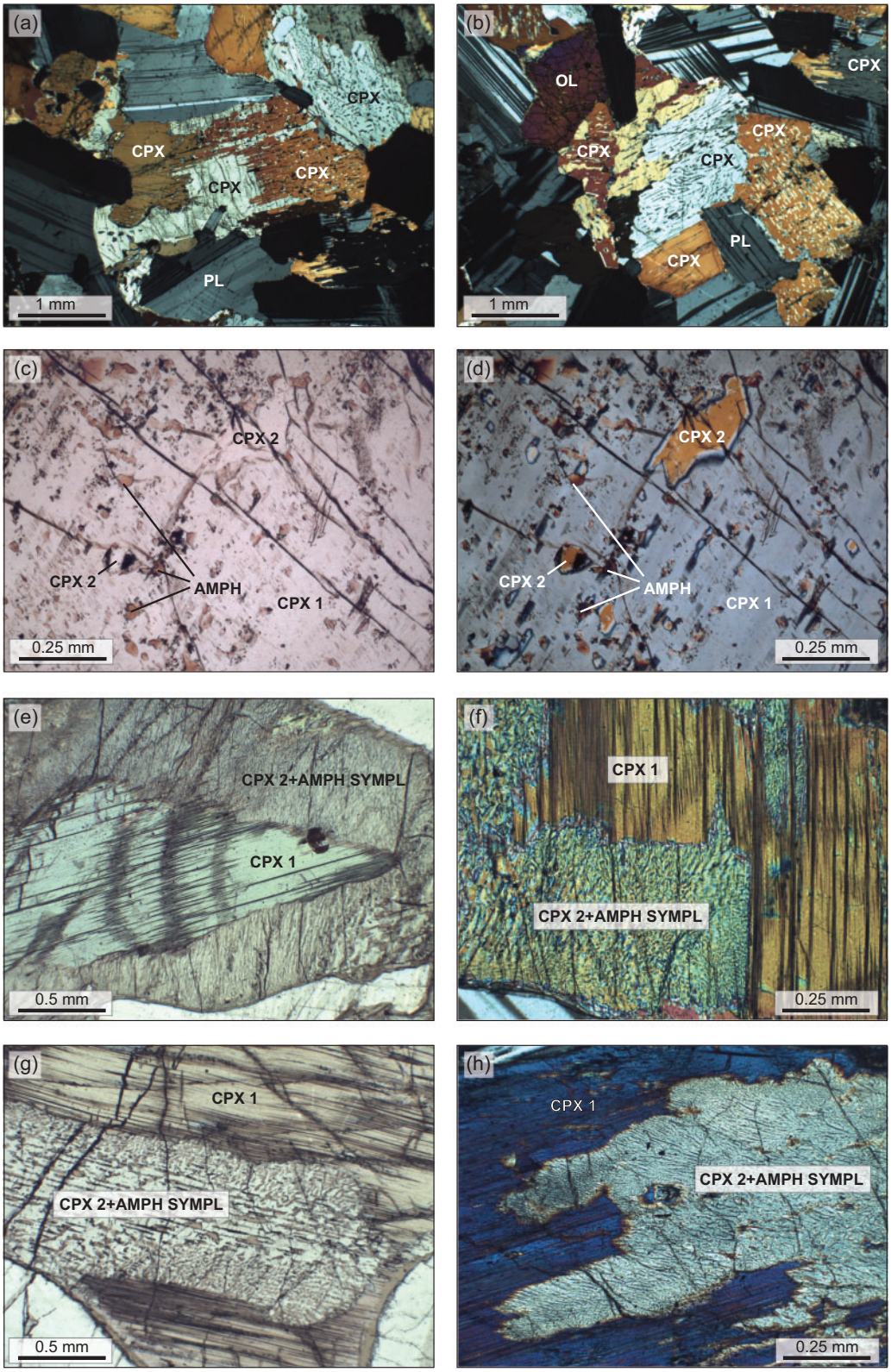

Fig. 2. Photomicrographs of clinopyroxene textures associated with RPF (all from ODP Hole 735B, Southwest Indian Ridge). (a, b) Irregular, ragged grain boundaries between a series of clinopyroxene crystals in olivine gabbro. (c, d) Brown amphibole blebs and associated secondary clinopyroxene in a large (~2 cm) cumulus clinopyroxene grain in olivine gabbro. (e–h) Examples of clinopyroxene–brown amphibole symplectites replacing clinopyroxene. AMPH, amphibole; CPX, clinopyroxene; CPX2 + AMPH SYMPL, clinopyroxene–amphibole symplectite; OL, olivine; PL, plagioclase.

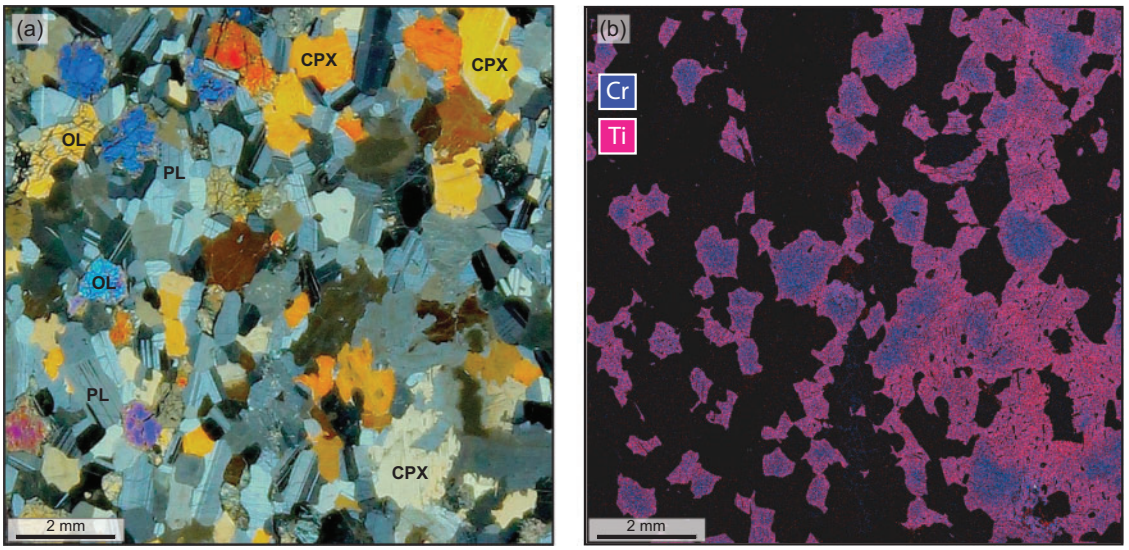

Fig. 3. Photomicrograph (a) and Cr–Ti element map (b) of primitive olivine gabbro JC21-70R-1 from Hess Deep (Pacific Ocean). A noteworthy feature is the granular, equilibrated cumulus texture, lacking evidence for reactions in (a) despite the clear cryptic zoning in Ti and Cr revealed by the element map in (b). The element map was obtained by a 300 mm^2 energy-dispersive spectrometry (EDS) system mounted on an field emission gun scanning electron microscope (FEG-SEM) (see Supplementary Data for details). CPX, clinopyroxene; OL, olivine; PL, plagioclase.

($\leq$2 kbar), MORB is not predicted to crystallize clinopyroxene until after significant olivine and plagioclase have crystallized (Grove *et al.*, 1992). As a result, the Mg# of the melt has already dropped significantly by the time clinopyroxene saturates, with experiments providing an average Mg# of 83 for the first clinopyroxene (Grove & Bryan, 1983; Tormey *et al.*, 1987; Grove *et al.*, 1990, 1992; Yang *et al.*, 1996). Clinopyroxene with higher Mg#s, which have commonly been found in oceanic gabbros (e.g. Elthon *et al.*, 1992), may represent formation at higher pressures ($P > 5$ kbar), where clinopyroxene saturation precedes that of plagioclase (Grove *et al.*, 1992). However, the high-pressure hypothesis is inconsistent with the rock record. In a case study on the Kane Megamullion gabbros, Lissenberg & Dick (2008) found that both the textures and mineral chemistry of the high-Mg# clinopyroxene (Mg# 86–91) require crystallization at low pressure from already evolved melts. Texturally, high-Mg# clinopyroxene encloses plagioclase or occurs as an interstitial phase between olivine and plagioclase, which indicates that the melt followed the normal low-pressure liquid line of descent, with olivine and plagioclase preceding clinopyroxene. Compositionally, the TiO_2 contents of the high-Mg# clinopyroxenes extend to very high values (1·46%), which indicates crystallization from evolved melts (Lissenberg & Dick, 2008). This is inconsistent with the early saturation of clinopyroxene required by high-pressure models. These observations can be reconciled by a model in which high-Mg# clinopyroxene forms as a result of reaction between migrating melts and a primitive olivine + plagioclase matrix [reaction (1) above; Meyer *et al.*, 1989; Lissenberg & Dick, 2008]. Because diffusive Fe–Mg exchange between olivine and melt is rapid (Chakraborty, 1997), melts migrating through a matrix containing primitive olivine will be buffered for Fe and Mg (Meyer *et al.*, 1989). Hence, upon crystallization, their clinopyroxene Mg# will be high, and exceed the Mg# expected on the basis of its actual degree of differentiation as indicated by TiO_2. Alternatively, gabbro assimilation may also produce melts with elevated Mg# (Kvassnes & Grove, 2008; Leuthold *et al.*, 2015). However, this would not produce the high TiO_2 observed, and is therefore unlikely to be important here.

Similarly complex relationships can be observed for clinopyroxene Cr_2O_3, which is high (up to 1·39%) in the Kane Megamullion samples, despite the fact that the same clinopyroxene TiO_2 indicates crystallization from melts with TiO_2 contents typical for moderately evolved MORB (Lissenberg & Dick, 2008). MORB Cr reaches a plateau at about 500 ppm, for which the equilibrium clinopyroxene contains ~0·5% Cr_2O_3 [for $D = 5{\cdot}9$, calculated for a primitive MORB composition using equation (627) of Bédard (2014)]. Hence, such high clinopyroxene Cr_2O_3 cannot be explained by fractional crystallization from MORB. The fact that the troctolite matrix in which these clinopyroxenes crystallized contains Cr-spinel, but that Cr-spinel is absent in the gabbroic bands with high-Mg#, high-Cr_2O_3 clinopyroxenes, suggests that Cr-spinel was removed by reaction during formation of the bands. This is in keeping with the predicted phase equilibria for MORB, which show that Cr-spinel is no longer on the liquidus when clinopyroxene saturates; hence, clinopyroxene-saturated melts are undersaturated in Cr-spinel. It follows that clinopyroxene-saturated melt flowing though a troctolite matrix would not only acquire a high Mg# but also dissolve its Cr-spinel, enriching the melt in Cr. The clinopyroxene crystallizing from the reacted melts will

thus have high Mg# and Cr, with only its TiO_2 content reflecting the true degree of differentiation of its parental melt.

The high-Mg, high-Cr signature of the Kane clinopyroxene can be readily observed elsewhere. In Fig. 4, we show clinopyroxene Mg#–Cr_2O_3–TiO_2 relationships for gabbroic (*sensu lato*) rocks from IODP Hole U1309D (Mid-Atlantic Ridge; data from Miller *et al.*, 2009). There is a significant population of high-Mg#, high-Cr_2O_3 clinopyroxenes (Fig. 4a). These clinopyroxenes form a distinct array in Cr–Ti space (Fig. 4b), maintaining high Cr_2O_3 concentrations at increasing TiO_2, even when TiO_2 concentrations increase to ~1%, which would suggest crystallization from a highly evolved melt (~2·4% TiO_2 assuming $D = 0{\cdot}42$ [D calculated from Bédard (2014) using mean composition of high-Mg#, high-Cr_2O_3 clinopyroxenes from Lissenberg & Dick (2008)]). Hence, although one might presuppose from the Mg#–Cr data that these clinopyroxenes represent grains crystallized from very primitive melts, their Cr_2O_3–TiO_2 relationships reveal that in fact the melts from which they formed were moderately to highly evolved. These relationships are the same as those in the well-studied Kane Megamullion sample of Lissenberg & Dick (2008), and we interpret the U1309D data in similar terms: melts that evolved to clinopyroxene saturation percolated through, and reacted with, a primitive olivine- and Cr-spinel-bearing matrix, leading to Mg#–Cr–Ti relationships unlike those expected in normal crystallization scenarios. This interpretation fits well with the fact that some of the high-Mg#, high-Cr_2O_3 clinopyroxenes occur in olivine-rich troctolites, which have previously been interpreted as hybrid rocks formed by melt percolation into peridotites (Suhr *et al.*, 2008; Drouin *et al.*, 2009, 2010). However, they are also abundant in rock types that form major building blocks of the lower oceanic crust (troctolite, olivine gabbro and some gabbro; Fig. 4).

Hence, we conclude that mineral major and minor element relationships may be significantly shifted away from those predicted by conventional models (i.e. those based on crystal–melt equilibrium) as a result of RPF. In the case of clinopyroxene, this results in the formation of what would commonly be interpreted as primitive and high-pressure crystals at low pressures and from evolved melts.

Mineral trace elements

Mineral trace elements are sensitive tracers of crystallization processes. Progressive fractional crystallization will lead to enrichment in incompatible trace elements, coupled with a decrease in compatible trace elements in both the melt and its crystallization products. The zoning patterns in crystals can be readily compared with fractional crystallization scenarios provided that accurate partition coefficients are available. In oceanic gabbros, mineral trace element studies to date have made a number of significant observations. First, clinopyroxene is commonly strongly zoned in trace elements. However, the core–rim enrichment in incompatible elements does not generally fit fractional crystallization models: highly incompatible trace elements are enriched beyond what is predicted by fractional crystallization relative to less incompatible trace elements (Coogan *et al.*, 2000; Gao *et al.*, 2007; Lissenberg *et al.*, 2013). There is a systematic relationship between the degree of this over-enrichment and the degree of incompatibility of a trace element in a gabbroic system (Lissenberg *et al.*, 2013). A prominent example is the over-enrichment of Zr to Nd: because the bulk partition coefficient of Zr in a gabbroic system is markedly lower (~0·06, reflecting the low Zr D in plagioclase) than that of Nd (bulk D of ~0·15), Zr is enriched more quickly than Nd, leading to an increase in Zr/Nd with progressive crystallization. This increase is greater than predicted by fractional crystallization, but can be reproduced by combined assimilation–fractional crystallization (AFC) models (Coogan *et al.*, 2000; Lissenberg *et al.*, 2013). Hence, the grain-scale over-enrichment in incompatible trace elements has been interpreted to result from dissolution–reprecipitation reactions between migrating melts and a crystal mush (Coogan *et al.*, 2000; Gao *et al.*, 2007; Lissenberg *et al.*, 2013).

Recently, Coogan & O'Hara (2015) argued that, instead of a reactive origin, the trace element distributions in oceanic clinopyroxene are controlled by diffusion. They envisaged that these crystals become initially zoned through crystallization of evolved trapped melts, and that the zoning patterns are then modified by diffusion to lead to the observed trace element fractionation. The diffusion of Zr, for example, was assumed to be significantly slower than Nd, leading to the increased Zr/Nd signature in the clinopyroxene rims that is so often observed (Coogan *et al.*, 2000). To test the reactive vs diffusion hypotheses for trace element zonation, we have acquired a detailed (170 points) laser ablation inductively coupled plasma mass spectrometry (LA-ICP-MS) core–rim traverse across a large clinopyroxene grain from an olivine gabbro from ODP Hole 735B (Fig. 5 and Supplementary Data Table 1; see Supplementary Data for analytical procedures; all supplementary data are available for downloading at http://www.petrology.oxfordjournals.org). This sample is typical of the dominant olivine gabbro lithology that forms the bulk of the 735B section, with a coarse-grained, granular texture (Fig. 5a). The selected clinopyroxene grain provides an ideal test case for the role of diffusion: it is sufficiently large (~1·5 cm) that diffusion cannot realistically have modified the trace element distributions across most of the crystal given the diffusion rates in clinopyroxene (e.g. Van Orman *et al.*, 2001) and the cooling rates prevalent in the lower oceanic crust (Coogan *et al.*, 2007). Moreover, an Fe–Mg–Na element map reveals that the grain is zoned in Fe–Mg (Fig. 5b), with a core Mg# of 84 and a rim Mg# of 70. Because Fe–Mg interdiffusion in clinopyroxene is significantly faster than diffusion of the relevant incompatible trace

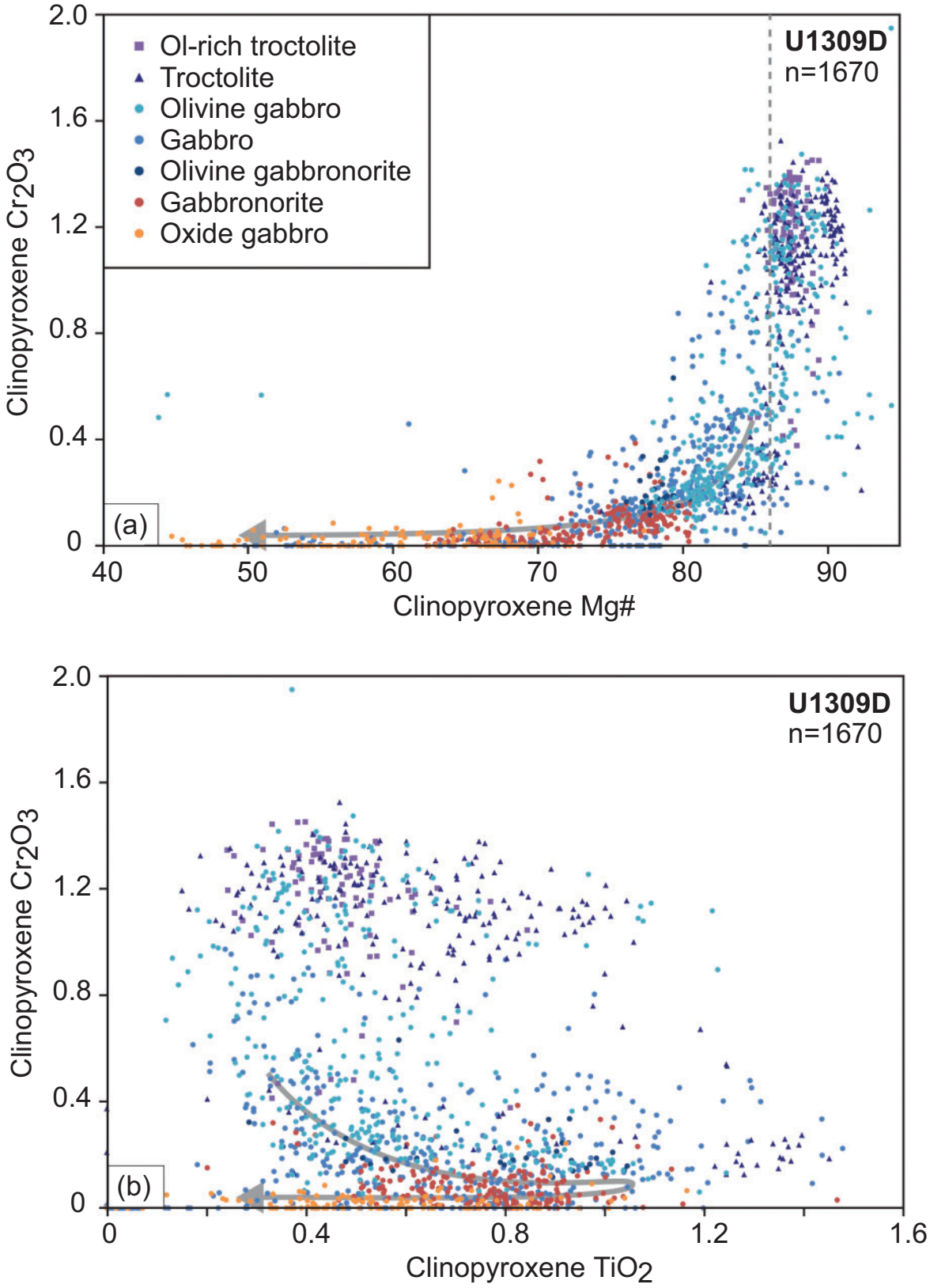

Fig. 4. Mg–Ti–Cr relationships in clinopyroxene from gabbroic rocks from IODP Hole U1309D at Atlantis Massif (Mid-Atlantic Ridge). (a) Mg#–Cr_2O_3. Dashed grey line separates a population of high-Mg clinopyroxene (Mg# > 86). (b) TiO_2–Cr_2O_3. Grey arrows mark schematic fractional crystallization trends of clinopyroxene in equilibrium with MORB undergoing fractional crystallization at low pressure. Data are from Miller *et al.* (2009), and are for 185 samples, covering the interval 32–1329 m below seafloor.

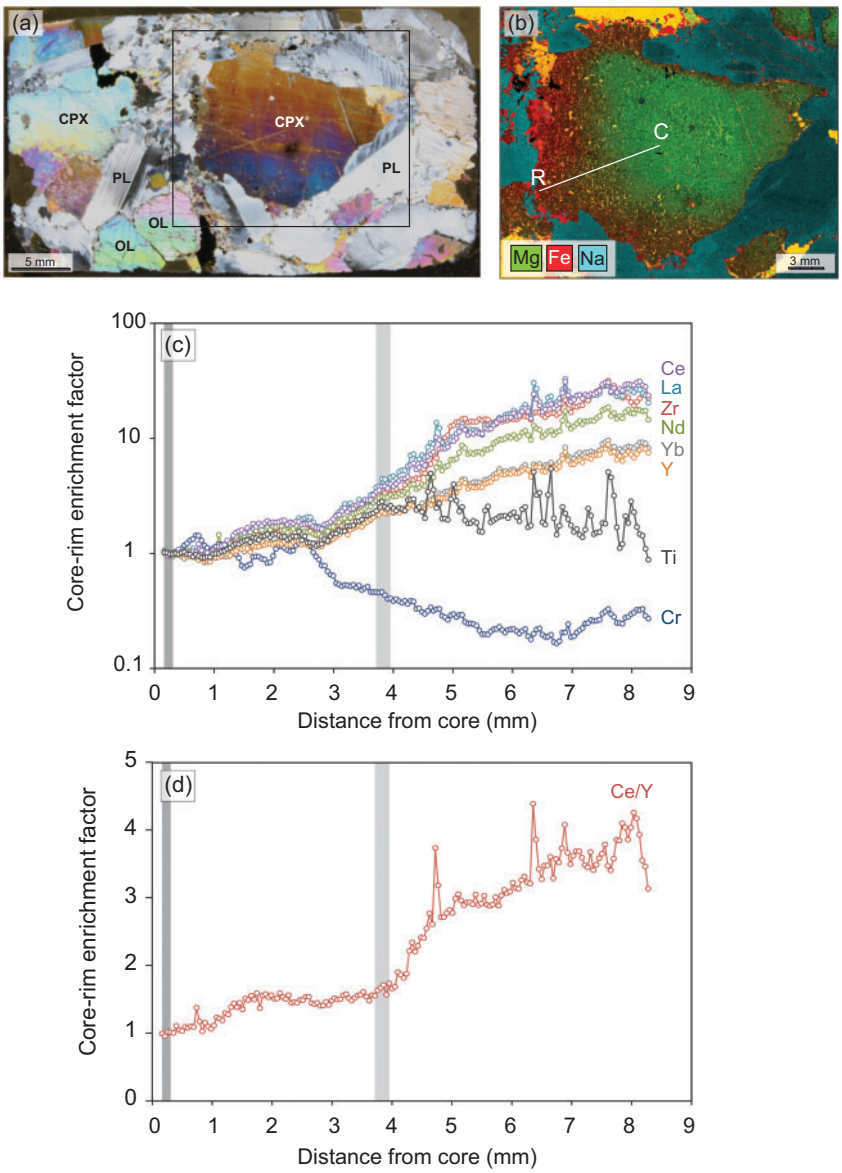

Fig. 5. Trace element distribution in clinopyroxene in olivine gabbro from ODP Hole 735B (Southwest Indian Ridge). (a) Full thin-section photomicrograph (crossed polars), with box outlining the area highlighted in (b). (b) Fe–Mg–Na element map of an analysed clinopyroxene crystal, showing the location of the laser ablation core–rim traverse. The zoning in Fe–Mg should be noted. Yellow inclusions in clinopyroxene are brown amphibole. Analytical technique is described in the Supplementary Data. (c) Enrichment factors (= concentration at given step divided by the core concentration) of Cr, Ti, Y, Yb, Nd, Zr, Ce and La. Irregular peaks, best displayed in Ti (e.g. at 4·7 mm and 6·3 mm), result from the beam overlapping minor inclusions, but do not appear to have a major effect on the overall profiles of the trace elements. Dark grey band outlines data point taken to represent the core; light grey band marks data points taken to represent enrichment prior to saturation of trace phases such as ilmenite. (d) Enrichment factor for the Ce/Y ratio.

elements (Dimanov & Wiedenbeck, 2006; Müller *et al.*, 2013), the preservation of Fe–Mg zoning provides a strong indication that the incompatible trace elements should preserve their original magmatic distributions. Hence, if the trace element distributions are controlled by RPF (see Lissenberg *et al.*, 2013) they will show the over-enrichment associated with this process. On the other hand, if the over-enrichment that is generally observed is produced by a diffusive overprint of enriched rims formed by fractional crystallization (Coogan & O'Hara, 2015), the trace element distributions in the 735B grain studied here should, in the absence of significant diffusion, follow a fractional crystallization pathway.

In Fig. 5c we show the core–rim distribution of selected trace elements (Cr, Ti, Y, Yb, Nd, Zr, Ce and La) in an ~8 mm core–rim traverse across the 735B clinopyroxene. These distributions are presented as enrichment factors: the concentration of an element at a given step relative to its concentration in the core. The grain is strongly zoned, with the enrichment in La, Zr and Ce reaching a factor of ~30. In terms of absolute

abundance, the core has a composition close to that of clinopyroxene in equilibrium with MORB (mean La = 0·17 ppm for the first four points), whereas the rim composition, which peaks at ~4·6 ppm, indicates growth from a strongly enriched melt. There is a significant difference in enrichment between La, Zr and Ce on the one hand and Y and Yb on the other (Fig. 5c). As a result, the Ce/Y ratio [the most precisely measured proxy for the degree of light to heavy rare earth element (LREE/HREE) fractionation in clinopyroxene owing to the high absolute concentrations of Ce and Y relative to the other LREE and HREE respectively] increases significantly from core to rim, showing an enrichment factor of ~4 (Fig. 5d). Zr/Nd increases to a maximum of ~1·9, although it decreases near the rim, where Zr concentrations show a slight dip. Ti shows a slight decrease in the second half of the profile, probably reflecting ilmenite saturation, which, along with the decrease in Mg# towards the rim, indicates that the melt that formed the rim was evolved beyond the point of oxide saturation.

Consistent with the presence of Fe–Mg zoning, we find no evidence for diffusion of the trace elements. There is a strong correlation between the enrichment of elements with different diffusion coefficients [e.g. Zr vs LREE vs middle REE (MREE)], such that increases and decreases in enrichment occur in the same place for these different elements [as also observed by Gao *et al.* (2007)]. Diffusion would lead to significant offsets in enrichment profiles between elements with different diffusivities. Furthermore, there is no decrease in La near the clinopyroxene rim, which would be predicted to occur if diffusion operated (Coogan & O'Hara, 2015). Hence, the data demonstrate that the trace element distributions are primary magmatic features. They do not, however, fit fractional crystallization trends. A fractional crystallization model for the interval of the grain that represents crystallization along the three-phase olivine–plagioclase–clinopyroxene cotectic (i.e. prior to ilmenite saturation; 0–3·9 mm), derived using cotectic proportions of olivine + plagioclase + clinopyroxene (0·075–0·435–0·49, respectively) and the partition coefficient compilation of Bédard (2001) is shown in Fig. 6. We first fit a fractional crystallization model to the measured Ce enrichment for this interval, and then examine whether the model fits the other elements. We find that, to match the Ce enrichment, 79% mineral fractionation (i.e. $F = 0{\cdot}21$) is required. It is clear, however, that the fractional crystallization model fails to provide a match for Y, which is lower than predicted (Fig. 6a). Similar to Zr/Nd, this is another example of the over-enrichment of more incompatible elements (Ce) relative to less incompatible ones (Y): the 79% fractional crystallization scenario only achieves a Ce/Y enrichment factor of 1·20, well short of the observed factor of ~1·7 (Fig. 6b). Hence, fractional crystallization cannot explain the trace element distributions in the first 3·9 mm of the profile. Moreover, fractional crystallization cannot, under any circumstances, produce the Ce/Y enrichment factor of >4 observed towards the clinopyroxene rim: even 99·9% fractionation ($F = 0{\cdot}001$) only increases the Ce/Y ratio by a factor of 2·3 (Fig. 6b). We therefore conclude that, although diffusion may play a role in small, slowly cooled grains, the over-enrichment in incompatible elements is a primary signature of a magmatic process that is more efficient than fractional crystallization at fractionating trace elements.

Coogan *et al.* (2000) and Lissenberg *et al.* (2013) successfully modelled the incompatible trace element over-enrichment using AFC models. Given that crystal–melt reactions are likely to operate by dissolution–reprecipitation (Liang, 2003), there is some justification for this approach. However, AFC models do not take into account the second significant finding of trace element studies of oceanic gabbros: that clinopyroxene cores (Lissenberg *et al.*, 2013) as well as plagioclase (Lissenberg *et al.*, 2013) and olivine (Drouin *et al.*, 2009; Sanfilippo *et al.*, 2014) may be strongly depleted in trace elements compared with what is expected of crystallization from MORB, although it should be pointed out that this depletion is not universal (e.g. the clinopyroxene core in Fig. 5 is in equilibrium with MORB). Because the degree of depletion in plagioclase (and to a certain extent olivine) correlates with partition coefficients, but

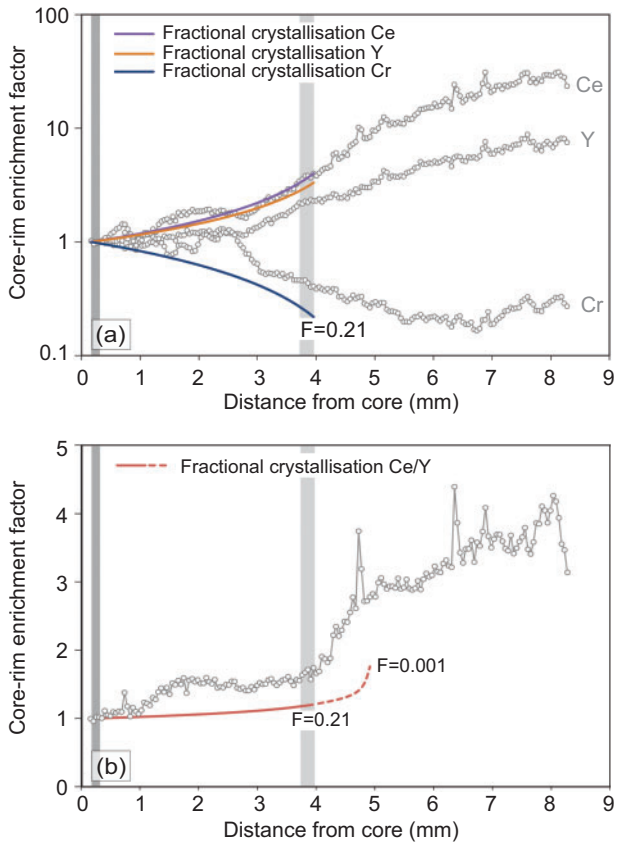

Fig. 6. (a) Fractional crystallization model superimposed upon the Cr, Y and Ce (a) and Ce/Y (b) data from Fig. 5, using partition coefficients compilation from Bédard (2001). It should be noted that fractional crystallization fails to reproduce the observed enrichments, even after 99·9% fractionation ($F = 0{\cdot}001$).

not diffusion coefficients (Lissenberg *et al.*, 2013), the process governing these distributions appears to be a magmatic one. Lissenberg *et al.* (2013) proposed that the depleted cores, where present, represent the residue of the reactions that generated the trace element enriched melts from which the clinopyroxene rims crystallized: as such, the enriched clinopyroxene rims are the trace element enriched counterpart to the depleted cores. If so, zone refining, a process by which a passing melt front depletes a solid framework in its impurities (i.e. incompatible elements) through (partial) melting (Pfann, 1952; Harris, 1957; McBirney, 1987), may be a more appropriate model to apply to oceanic gabbros. We model zone refining using the equation from (Harris, 1957):

$$\frac{C_L}{C_0} = \frac{1}{D} - \left(\frac{1}{D} - 1\right)e^{(-Dl)} \quad (1)$$

where C_L is the concentration of an element in the liquid after zone refining, C_0 is the initial concentration of that element in the liquid, D is its partition coefficient, and l is the number of equivalent volumes of solids processed by the liquid. However, the choice of appropriate values for these input parameters is not straightforward; there is significant uncertainty on both l and the mineral modes and any potential modal changes associated with zone refining, which makes it difficult to select appropriate partition coefficients. We have therefore modelled three scenarios, covering different l and different mineral modes (Fig. 7). To test whether zone refining may explain the trace element enrichment observed in the 735B clinopyroxene from Fig. 5 we compare the enrichment in trace elements (i.e. C_L/C_0) of the zone refining models with the clinopyroxene data (Fig. 7). As before, we have taken the enrichment in the analysed clinopyroxene crystal to the point of saturation of trace phases (outlined by the grey box in Fig. 5) to focus on melt evolution in a cotectic olivine–plagioclase–clinopyroxene system. Despite the uncertainty relating to l and phase proportions during zone refining, the correlation between zone refining and the natural clinopyroxene data is significant in all models ($R^2 = 0{\cdot}83$–$0{\cdot}95$; Fig. 7). Hence, the over-enrichment of trace elements in clinopyroxene relative to fractional crystallization (as illustrated in Fig. 5) is similar to that expected to develop during zone refining of a gabbroic system. This is consistent with the hypothesis that RPF in oceanic magma chambers occurs though a process akin to zone refining (Lissenberg *et al.*, 2013).

In summary, the crystal-scale distributions of trace elements in oceanic gabbros appear to be controlled by a type of reactive process that redistributes trace elements, over-enriching the melts in incompatible elements relative to fractional crystallization.

Sample scale

Oceanic gabbroic rocks are commonly complex on a sample scale. Excellent examples are provided by cores recovered by ocean drilling, which commonly contain different gabbroic rock types with complex relationships on a small (centimetre to decimetre) scale. Element mapping is an excellent tool to investigate such complexities, and we here present two examples from Hole 735B (Fig. 8; see Supplementary Data for method). The first is from a fine-grained troctolite unit, which contains strings of medium-grained olivine gabbro (Fig. 8a and b). The contact between the two lithologies ranges from diffuse to moderately sharp. The Fe–Mg–Na element map of a thin section containing a troctolite–olivine gabbro–troctolite profile reveals that there is a continuous gradation in Fo content of the olivine from the troctolite (Fo_{80}) to the olivine gabbro (Fo_{70}). Furthermore, the An content of plagioclase in the troctolite (An_{72}) is higher than that of the olivine gabbro (as low as An_{54}). Critically, some plagioclase crystals in the olivine gabbro preserve resorbed cores of higher An plagioclase that is similar to that of the host troctolite, and small, high-Mg# clinopyroxene grains (Mg# 87) occur in the top left corner of the troctolite. The occurrence of high-Mg clinopyroxene in the troctolite indicates that the olivine gabbro is unlikely to simply be a vein in the troctolite, even if Fe–Mg diffusion during and/or after intrusion is invoked to produce the Fo gradient. This is because, like their Kane counterparts, the high-Mg# clinopyroxene occurs together with olivine and plagioclase, and therefore cannot have formed by fractional crystallization, requiring formation through reaction with the troctolite olivine instead (see above). Together, the observations imply that a three-phase saturated melt percolated through the troctolite, resorbing the anorthitic plagioclase of its host, and crystallizing lower-An plagioclase, lower-Fo olivine and clinopyroxene. Percolation of small volumes of intergranular melt into the troctolite matrix formed the small high-Mg clinopyroxene crystals. Fe–Mg diffusion between the percolating melt and the olivine of the troctolite lowered the Fo contents of the troctolite olivine, generating the observed Fo gradient. Hence, the olivine gabbro strings formed through reactive porous flow of a more evolved and clinopyroxene-saturated melt through the troctolite. This is consistent with the irregular nature of the strings as revealed by core observations (Fig. 8a).

A second example of complex sample-scale relationships is provided in Fig. 8c and d. This medium-grained olivine gabbro contains a narrow (0·5–1 cm) oxide gabbro mylonite band: one of the hallmarks of the 735B section (Dick *et al.*, 2000; Natland & Dick, 2001). The contact in hand specimen appears to be sharp (Fig. 8c). An Mg–Fe–Na–P element map (Fig. 8d) reveals that the oxide gabbro contains markedly lower An plagioclase and clinopyroxene Mg# (An_{25}, Mg# 71) compared with its host (An_{43}, Mg# 78), which is consistent with its high mode of Fe–Ti oxides and apatite. However, the oxide gabbro contains relict resorbed cores of plagioclase with An contents similar to that of the olivine gabbro. Furthermore, the cumulus clinopyroxene in the olivine

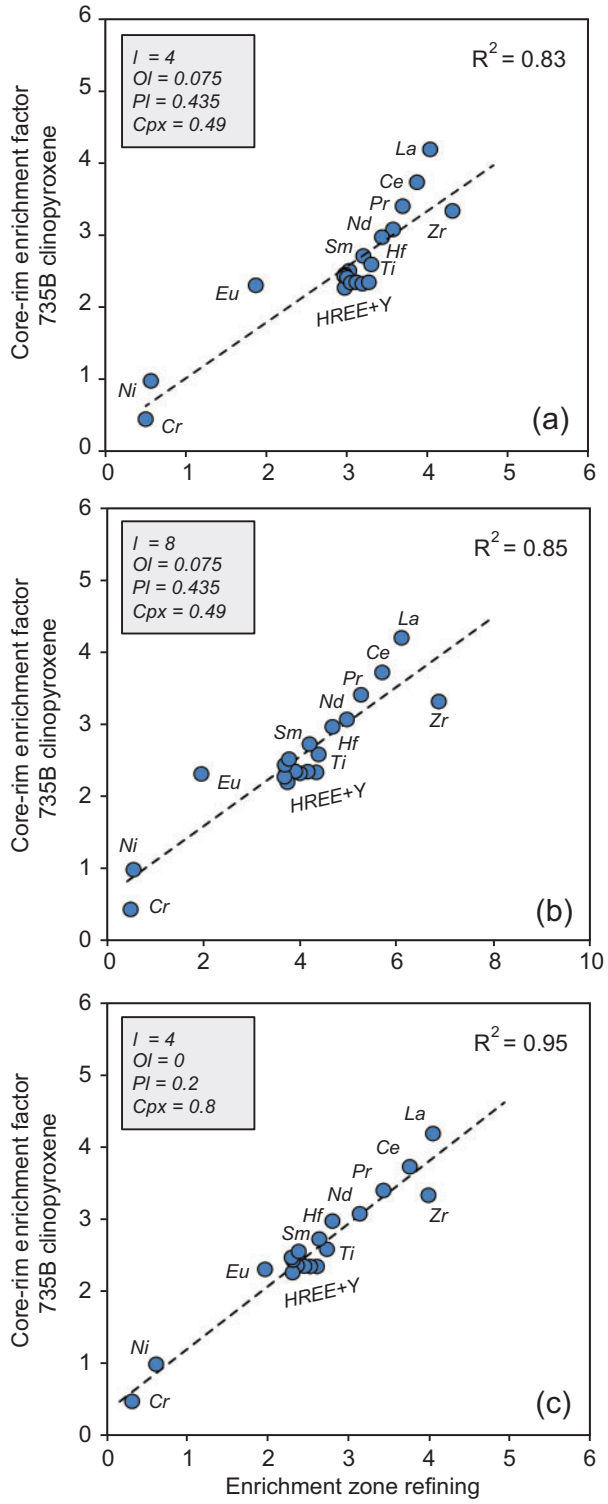

Fig. 7. Correlation between three zone refining scenarios and the trace element enrichment observed in clinopyroxene from Fig. 5. Zone refining parameters are outlined in the grey box (*I* is the number of equivalent volumes of solids processed by the liquid; Ol, Pl and Cpx are the proportions of olivine, plagioclase and clinopyroxene in gabbro subject to zone refining). Trace element enrichment in clinopyroxene is taken for the interval of the grain that represents crystallization along the three-phase olivine–plagioclase–clinopyroxene cotectic (i.e. prior to ilmenite saturation, outlined by the grey box in Fig. 5). Partition coefficients used in the zone refining model are from the compilation of Bédard (2001).

gabbro is zoned in Fe–Mg: low Mg# rims (Mg# 74), which are invaded by small brown amphibole blebs similar to those shown in Fig. 2d, are intermediate between the core (Mg# 78) and the clinopyroxene in the oxide gabbro (Mg# 71). These relationships require that a highly evolved melt infiltrated the olivine gabbro and reacted with its constituent minerals to produce the oxide gabbro. The integrated melt flux was high in the centre of the sample, leading to an evolved, Fe–Ti oxide- and apatite-rich oxide gabbro with completely re-equilibrated clinopyroxene, and low towards the edges of the sample, leading to zoning of cumulus clinopyroxene, with the formation of low-Mg#, amphibole-bearing reaction rims, plus An zoning of cumulus plagioclase (Fig. 8d). Similar to the example of the olivine gabbro string in the troctolite (Fig. 8a and b), porous flow of melt through a plutonic rock has fundamentally changed its mineralogy and composition.

These two examples illustrate that RPF may be responsible for the evolution of plutonic rocks, at least on a sample scale. In both cases, it has transformed one rock type into another, and was the dominant control on the An–Fo–cpx Mg# relationships. By extension, it would have had a significant effect on the compositions of the melts involved. Literature data suggest that these cases are far from unique. Other well-described examples include the following: (1) the formation of olivine-rich troctolites by the infiltration of migrating melts into the olivine framework of mantle peridotites in both oceanic (Suhr *et al.*, 2008; Drouin *et al.*, 2009, 2010; Sanfilippo *et al.*, 2015*a*) and ophiolitic sections (Sanfilippo *et al.*, 2014); (2) the transformation of troctolite into gabbro in rocks from the Kane Megamullion (Lissenberg & Dick, 2008).

Lower crustal scale

To constrain the length scale over which RPF operates we examine the clinopyroxene trace element distributions within two stratigraphic sections through the lower crust. Because only one more or less complete section through lower crust is available in the oceans (Hess Deep; Lissenberg *et al.*, 2013), we also include a section through the lower crust of the Oman ophiolite (Wadi Abyad; MacLeod & Yaouancq, 2000; Coogan *et al.*, 2002*b*; Thomas, 2003). This section samples gabbroic rocks that formed during the main axial stage of crustal growth (Geotimes unit), whose magmas, with the exception of elevated water contents, were MORB-like (Godard *et al.*, 2006; MacLeod *et al.*, 2013). Although the nature of the reaction processes may be influenced by the elevated water contents of the magmas, our purpose in this section is to examine the scale, not the exact nature, of RPF. Given that the physical parameters that govern melt migration and mush compaction (melt fraction, permeability, viscosity, buoyancy of melt relative to solid) are likely to be similar between Oman and a mid-ocean ridge magma chamber, we

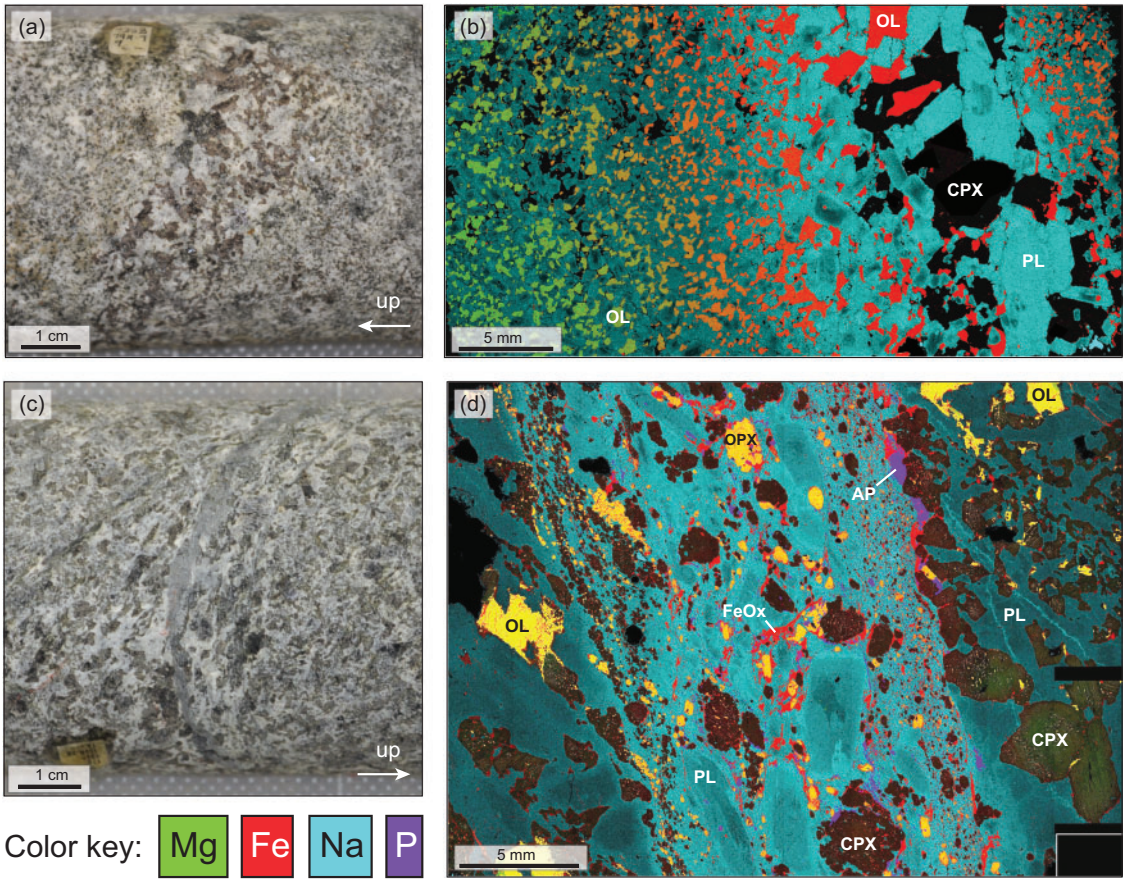

Fig. 8. Core photos (a, c) and Mg–Fe–Na (b) and Mg–Fe–Na–P (d) element maps of two samples from ODP Hole 735B. (a, b) Fine-grained troctolite with medium-grained olivine gabbro string (sample 735B-79R-7, 104–108 cm). The decrease in Fo and An content of olivine and plagioclase (green to red and dark to light shade of blue, respectively) towards olivine gabbro should be noted. Clinopyroxene appears black because Fe and Mg have been scaled to show the olivine compositions. (c, d) Medium-grained olivine gabbro with oxide gabbro shear band (sample 735B-150R-3, 8–11 cm). Noteworthy features are the decrease in clinopyroxene Mg# and An content of plagioclase (green to red and dark to light shade of blue, respectively) from olivine gabbro to oxide gabbro, the relict cores of relatively anorthitic plagioclase in oxide gabbro, and the mode of Fe–Ti oxides and apatite in the oxide gabbro. Olivine and orthopyroxene appear yellow to orange because Fe and Mg have been scaled to show the clinopyroxene compositions. AP, apatite; CPX, clinopyroxene; FeOX, Fe-oxide; OL, olivine; OPX, orthopyroxene; PL, plagioclase. Analytical protocol for EDS element mapping is described in the Supplementary Data.

consider using Oman as a second case study for the scale on which RPF operates, to be justified.

The stratigraphic variation of clinopyroxene chondrite-normalized (Anders & Grevesse, 1989) Ce/Y ratios is illustrated in Fig. 9. Although there is considerable complexity at any given level owing to large grain-scale variations in trace element ratios (see mineral trace element section above), there appears to be an overall increase in clinopyroxene Ce/Y between different stratigraphic levels. It is low (averaging ~0·2 at Hess Deep and ~0·15 in Oman) in the lower half of the crust, where primitive layered gabbros are exposed in both sections (MacLeod & Yaouancq, 2000; Lissenberg *et al.*, 2013; Gillis *et al.*, 2014). The ratio then increases, particularly at Hess Deep, in the overlying gabbros, which generally exhibit a marked foliation that is steeply dipping both in Oman (Boudier *et al.*, 1996) and Hess Deep (ODP Hole 894G; MacLeod *et al.*, 1996). Another step increase in clinopyroxene Ce/Y (to ~0·35 at Hess Deep and ~0·25 in Oman) occurs in the top few hundred metres, where evolved, isotropic gabbroic rocks are exposed in both Oman (MacLeod & Yaouancq, 2000; Coogan *et al.*, 2002*b*) and Hess Deep (Lissenberg *et al.*, 2013). Hence, both sections show an up-section increase in clinopyroxene Ce/Y by a factor of around 1·6–1·7. We note that this is a minimum: at least at Hess Deep, the common occurrence of apatite in the isotropic gabbros indicates that melts at this level reached apatite saturation, which would have decreased Ce/Y, accounting for the lower end of the Ce/Y range observed at this level.

The up-section increase in clinopyroxene Ce/Y could be due to either variations in the degree of LREE depletion of the parental melts to the sections (i.e. a mantle signature) or crustal-level differentiation processes, and the same is true for the grain-scale variations in trace element ratios (Fig. 5d). If the mantle generates both LREE-depleted [normal (N)-MORB] and LREE-enriched [enriched (E)-MORB] melts, each would be expected to form a series of primitive-to-evolved cumulates, generating a series of subhorizontal trends in Harker

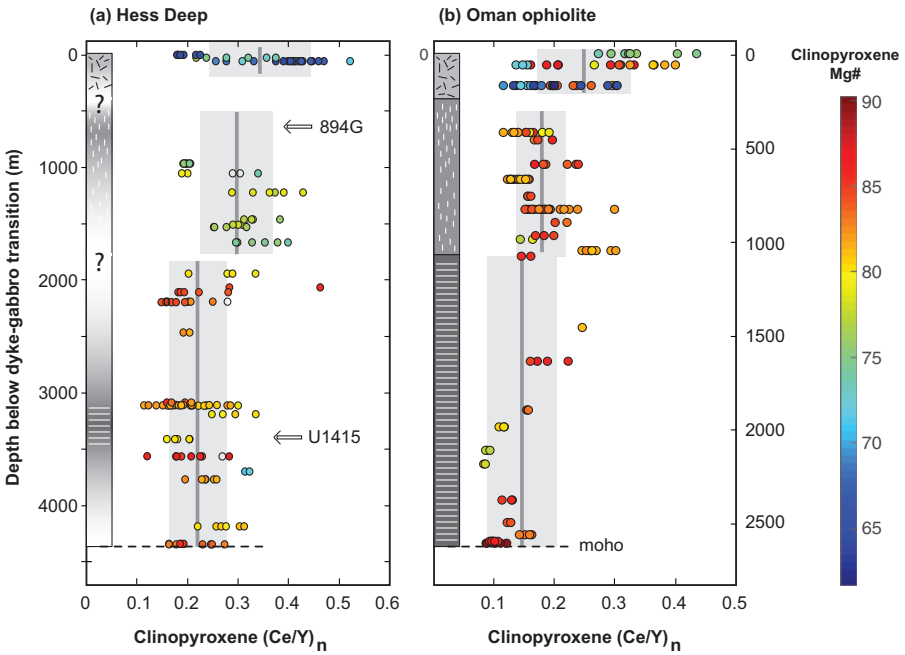

Fig. 9. Clinopyroxene chondrite-normalized Ce/Y ratios vs depth below the dyke–gabbro transition zone for Hess Deep (a) and the Wadi Abyad section of the Oman ophiolite (b). The data are color coded for clinopyroxene Mg#, with the scale displayed to the right of the figure. Grey lines mark the mean ratios of three stratigraphic levels, with the light grey box outlining the standard deviation. The increasing average Ce/Y with stratigraphic height indicates that, despite complexities on a crystal scale to hundreds of metres scale (reflected in the relatively large standard deviations), there is an overall up-section increase in clinopyroxene Ce/Y. In Oman, these three levels comprise (from bottom to top) the layered gabbros (dark grey), foliated gabbros (grey) and isotropic gabbros (light grey) (MacLeod & Yaouancq, 2000). In Hess Deep, (I)ODP drilling and remotely operated vehicle (ROV) sampling indicate that a similar stratigraphy is present (layered gabbros at Site U1415: Gillis *et al.*, 2014; foliated gabbros with steep fabrics in Hole 894 G: MacLeod *et al.*, 1996; isotropic gabbros in the top ~100 m: Lissenberg *et al.*, 2013). Samples from expedition JC-21 presented here are consistent with the observations in the drill holes, and define three levels with markedly different mineral compositions (Lissenberg *et al.*, 2013). The mean clinopyroxene Ce/Y shown here therefore uses this three-fold subdivision. Data points represent single spot analyses, and are taken from Lissenberg *et al.* (2013) (Hess Deep) and Coogan *et al.* (2002*b*) and Thomas (2003) (Wadi Abyad).

diagrams (e.g. Ce/Y vs Mg#; Fig. 10). In this scenario, magma mixing during cumulate formation may result in cumulates with intermediate trace element signatures, as well as cumulate grains zoned in trace elements. However, there are three arguments against this scenario. First, there is no evidence of distinct series of cumulates (Fig. 10). Instead, the data show that Ce/Y increases with decreasing Mg# (Fig. 10). This inverse correlation covers a large range of Mg#, and is present both on a grain scale (Mg# 84–70: Fig. 5) as well as a stratigraphic scale (e.g. Hess Deep, Mg# 88–65: Figs 9 and 10). Second, rims are systematically more enriched than cores, which would not be expected if the trace element zoning was due to mixing: mixing would occur in both directions (i.e. N-MORB rims on E-MORB cores and vice versa), which is not observed. Third, there is no apparent reason why melts with higher Ce/Y ratios should be emplaced systematically higher in the crust, and that this pattern would be present at Hess Deep as well as Oman. Hence, the data do not support a mantle control on incompatible trace element distributions. Instead, the fact that the enrichment develops upwards through the lower crust and is coupled with decreasing Mg# provides strong evidence that it is a differentiation-controlled feature. However, the data indicate that this differentiation process is not fractional crystallization. As shown above, fractional crystallization is not very efficient in fractionating Ce from Y. We model the up-section Ce/Y fractionation at Hess Deep by taking the average anorthite content of plagioclase from the deep (>1800 m below dyke–gabbro transition; Fig. 9a) and shallow (<250 m) levels of the Hess section (An = 76·6 and 52·7, respectively; data of Lissenberg *et al.*, 2013), and relating these to melt mass of a fractional crystallization path of a primary East Pacific Ridge (EPR) magma. The latter was derived by regression of the PetDB EPR dataset (Lehnert *et al.*, 2000), and is provided in Table 1 (see Supplementary Data for details). The fractional crystallization path, modelled using MELTS (Ghiorso & Sack, 1995) at pressure of 1·5 kbar, oxygen fugacity of QFM − 1 (where QFM is quartz–fayalite–magnetite buffer) and an assumed H_2O content of 0·15 %, indicates that the difference in plagioclase anorthite content between the deep and shallow levels at Hess Deep records 50·4% mineral fractionation. Assuming Ce and Y bulk *D* values of 0·12 and 0·23, respectively [again using cotectic proportions and *D* values from Bédard (2001)], it follows that fractional crystallization would have increased the Ce/Y ratio by a factor of 1·16. The same exercise using the Mg# of clinopyroxene (average Mg# 84 in the deep gabbros, 70 in shallow gabbros; Lissenberg *et al.*, 2013) instead of the anorthite content

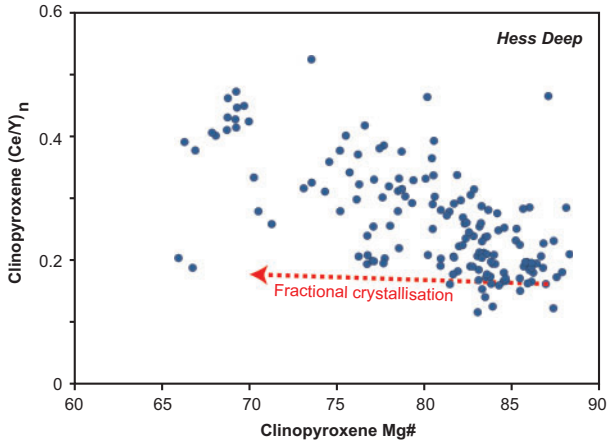

Fig. 10. Relationship between clinopyroxene Mg# and chondrite-normalized (n) Ce/Y ratio for the lower crustal section exposed at Hess Deep. Also shown is a fractional crystallization pathway (red) for clinopyroxene in equilibrium with MORB, with a primitive Hess Deep clinopyroxene core as the starting composition. The fractional crystallization trend was derived from a MELTS model of the primary EPR MORB presented in Table 1. Mineral modes along the liquid line of descent predicted by MELTS were used to calculate bulk *D* values for Ce and Y at each step, allowing the Ce and Y evolution of the melt to be determined. Clinopyroxene Ce/Y values were then calculated from melt Ce/Y using the partition coefficients of Bédard (2001). Data from Lissenberg *et al.* (2013).

Table 1: East Pacific Rise primary MORB

SiO_2	49·5
TiO_2	0·87
Al_2O_3	17·0
FeO	6·75
Fe_2O_3	0·75
MnO	0·15
MgO	9·80
CaO	12·5
Na_2O	2·40
K_2O	0·05
P_2O_5	0·08
H_2O	0·15
Total	100·00
Mg#	72·1
CaO/Na_2O	5·2

of plagioclase yields a Ce/Y fractionation factor of 1·13. Although there is inherent uncertainty in these models, both factors fall well short of the observed fractionation factor of 1·6–1·7. Hence, the trace elements in the lower oceanic crust are controlled by a differentiation process that is more effective than fractional crystallization at fractionating trace elements.

Similar to the grain-scale zoning presented above (Fig. 5), the ratio of Ce/Y examined here reflects a broader observation: that any incompatible element is enriched up-section more at a given amount of fractionation relative to less incompatible elements compared with fractional crystallization models (Lissenberg *et al.*, 2013). In other words, more-to-less incompatible elements in the Hess Deep and Oman gabbroic rocks are systematically over-enriched up-section. Because the same enrichment signature is present from core to rim, Lissenberg *et al.* (2013) argued that the same process was responsible for both the core–rim and up-section distribution of trace elements. The arguments presented by Lissenberg *et al.* (2013), and reiterated above, indicate that this process was RPF. Hence, the fact that the incompatible trace element ratios increase throughout the entire lower crust, and that this observation holds for both Hess Deep and the Oman ophiolite, indicates that RPF occurred on the scale of the entire lower crust.

THE LINK TO MORB

If RPF occurs on a lower crustal scale, this raises the question of whether it plays a role in the petrogenesis of MORB. The major element perspective of this question was addressed by Lissenberg & Dick (2008). Their detailed study of the Kane Megamullion samples (see section on 'textures') indicated that the generation of gabbroic bands in troctolite is governed by the reaction of melt with olivine, high-An plagioclase and Cr-spinel to generate clinopyroxene + low-An plagioclase [reaction (1) above]. The element map showing the transformation of a Hole 735B troctolite into olivine gabbro (Fig. 8a and b) is fully consistent with this reaction: clinopyroxene precipitates in the olivine gabbro band, and relatively anorthitic plagioclase is resorbed, being replaced by lower-An plagioclase. Reaction (1) is not the only reaction occurring in gabbroic crystal mushes, as evidenced, for example, by the clinopyroxene–amphibole symplectites [reaction (2)]. However, the symplectites appear to occur mainly on a grain scale (Fig. 2) and may result from local reaction of evolved melt at relatively small melt fractions. In contrast, reaction (1) occurs in channels, and extends to relatively large scales (at least outcrop scale; Lissenberg & Dick, 2008, fig. 12). Furthermore, its hallmark signature (high-Mg# clinopyroxene) is a common constituent in oceanic gabbros (e.g. Fig. 4). Hence, it is likely to be an important reaction in oceanic magma chambers during melt transport.

Because plagioclase occurs on either side of this reaction (albeit with a different composition), the net modal change effected by the transformation of troctolite into olivine gabbro is the replacement of olivine by clinopyroxene. The effect of this reaction on the full major element inventory of the melt was modelled by Lissenberg & Dick (2008); Cr was not included, because the small proportion of spinel assimilated means that it does not significantly affect the major elements. The main findings were that the melt shifts in composition to lower CaO and higher Al_2O_3, and that melt MgO increases. Combined, this leads to a compositional shift away from the low-pressure liquid line of descent that is very commonly observed in MORB: a shift towards higher MgO at a given CaO (e.g. Lissenberg & Dick, 2008, fig. 10). Previously, this spread was interpreted to represent a difference in the pressure of fractional crystallization (Grove *et al.*, 1992; Danyushevsky *et al.*, 1996; Michael & Cornell, 1998; Herzberg, 2004; Villiger *et al.*,

2007): at elevated pressures, the clinopyroxene stability field expands relative to that of plagioclase, leading to earlier clinopyroxene fractionation and hence a CaO decrease at relatively high MgO. Hence, the MORB liquid lines of descent were parameterized for pressure of fractionation, showing that pressures of up to 8 kbar are common (Grove *et al.*, 1992; Danyushevsky *et al.*, 1996; Michael & Cornell, 1998; Herzberg, 2004; Villiger *et al.*, 2007). According to these parameterizations, a large majority (72%) of glasses from the Mid-Atlantic Ridge would have last crystallized in the upper mantle prior to eruption, with a large peak at ~4 kbar or ~12 km, resulting in an average of 17–19% gabbroic ($P < 5$ kbar) and ultramafic ($P > 5$ bar) cumulates in the upper mantle (Lissenberg *et al.*, 2013). There are a number of problems with this interpretation. First, it is inconsistent with the rock record. Mantle sections, where recovered, do not typically show a large proportion of cumulate rocks. Furthermore, olivine melt inclusion CO_2–H_2O relationships indicate that the deepest crystallization occurs at ~9 km (~3 kbar) below the seafloor at slow (Wanless *et al.*, 2015) and even ultraslow-spreading ridges (Shaw *et al.*, 2010), where crystallization would be predicted to be deepest. Finally, at oceanic core complexes, which represent melt-poor lithospheric accretion along slow-spreading ridges, and which in at least some cases comprise gabbroic plutons embedded in mantle peridotites (e.g. Kelemen *et al.*, 2004), crystallization depths have been shown to be ~6–8 km, equivalent to ~2–3 kbar (Grimes *et al.*, 2011; Schoolmeesters *et al.*, 2012; Lissenberg *et al.*, 2016). Second, is not clear how melts would be erupted from depths of up to ~25 km, as implied by the pressure calculations, without further increments of crystallization or mixing. On the basis of these arguments, and because the shift in melt composition during reactive formation of clinopyroxene-rich lithologies from olivine-rich ones matches the shift in MORB compositions, Lissenberg & Dick (2008) proposed that the MORB array reflects, at least in part, RPF in lower crustal magma chambers. The common occurrence of high-Mg# and high-Cr clinopyroxene (Fig. 4), and the fact that the troctolite-to-olivine gabbro reactions have now also been observed in the Hole 735B section (Fig. 8), lend further support to this contention.

Regarding trace elements, we have shown above that RPF produces an over-enrichment of more relative to less incompatible elements when compared with fractional crystallization predictions, and that this signature occurs both on a grain scale (Fig. 5) and on a lower crustal scale (Fig. 9). O'Neill & Jenner (2012) presented the trace element distributions of a global suite of ocean floor basalts, and similarly found that incompatible trace elements are more enriched and fractionated than can be accomplished by fractional crystallization. Lissenberg *et al.* (2013), focusing on Ce and Y, demonstrated that this is also the case for the PetDB EPR dataset (their fig. 9).

Here, we explore to which extent the incompatible trace element enrichment in the lower crustal rocks matches that observed in MORB. To this end, we compare the enrichment in the detailed core–rim profile in the Hole 735B olivine gabbro (Fig. 5) with the global ocean floor basalt trace element distributions (O'Neill & Jenner, 2012). These trace element distributions reflect the crustal evolution of mantle melts. The parameterization of a large suite of trace elements versus MgO provided by O'Neill & Jenner (2012) allows the crustal evolution of ocean floor basalts to be calculated. Using this parameterization, we calculate the enrichment in the global trace element dataset between 8·6 and 5·6 wt % MgO, which represents the window in which the O'Neill & Jenner (2012) model to account for the trace element distributions reaches steady state. It should be noted that the result of our comparison is independent of the chosen MgO window: it is the slopes of the trace element data versus MgO that are relevant for comparison with the clinopyroxene data. For the 735B clinopyroxene profile, we calculate the enrichment to be from the crystal core to the point of saturation of Fe–Ti oxides (light grey box in Fig. 5), to focus on melt evolution in a three-phase saturated system and to avoid the uncertainties introduced on the partition coefficients by the saturation of trace phases such as ilmenite. The results are shown in Fig. 11. The correlation between the trace element enrichment in the 735B clinopyroxene and that observed in ocean floor basalts is very strong ($R^2 = 0{\cdot}97$), which demonstrates that the trace element distributions in ocean floor basalts are consistent with an origin by RPF in the lower crust.

DISCUSSION

How common is reactive porous flow?

Above, we have shown that RPF can play an important role in the evolution of oceanic plutonic rocks, and that the resulting major and trace element distributions are similar to those in MORB. To assess whether RPF represents a bona fide candidate for controlling MORB compositions we need to establish not only its scale (Fig. 9), but also its extent. In Fig. 12, we compile the existing trace element data for clinopyroxene from the lower oceanic crust. Focusing once again on Ce–Y relationships during differentiation, in Fig. 12 we show the global array in clinopyroxene Ce–Y, as well as fractional crystallization and zone refining predictions for comparison. The data reveal two important observations. First, the global clinopyroxene array shows much stronger enrichment in Ce relative to Y than fractional crystallization can account for, mimicking the grain-scale observations in Fig. 5. In contrast, zone refining can generate the observed over-enrichment in Ce relative to Y, with additional fractional crystallization of resulting melts required to reproduce the evolved end of the global data array. Second, the observation of Ce over-enrichment holds for samples from the three main ocean basins (Pacific, Atlantic and Indian Oceans). Hence, the signature of RPF is a general feature in the lower oceanic crust. The observation that trace element

fractionation correlates inversely with Mg# (Fig. 10) indicates that RPF is an inherent part of the differentiation process in oceanic magma chambers.

An important role for RPF fits well with theoretical considerations on crystal mush evolution. Recently, Solano *et al.* (2014) developed a quantitative model of a crystal mush undergoing compaction, which included heat, mass and major and trace element transport and reaction. They made two significant findings that are relevant here. The first is that melt migrating through a compacting crystal mush will react with the mush. Critically, they found that melts migrating through a homogeneous mush column, as well as melts in sill-like bodies cooled from above and below, acquire an enriched trace element signature. Similar to the observations in gabbros (Lissenberg *et al.*, 2013), the enrichment in incompatible elements exceeds that predicted by conventional models. The second finding is that melt migration through a crystal mush may lead to the formation of high-porosity melt layers. This provides a mechanism for reacted melts to concentrate and, owing to the instability of melt-rich zones in a compacting mush, to escape upwards. An additional mechanism of extracting reacted interstitial melts from the crystal mush is its destabilization by small amounts (10–20%) of partial melting (Huber *et al.*, 2011). Given that the emplacement of hot, primitive melt into crystal mush is likely to be a common process at mid-ocean ridges, partial melting and the resulting unlocking of the surrounding crystal mush could potentially occur. In conclusion, the available models for crystal mush evolution indicate that crystal mushes are inherently reactive, and that reacted melts may be extracted from them.

The parallels between these physico-chemical models of crystal mush evolution and the pervasive reaction in oceanic magma chambers revealed by the natural data are striking. The model predictions of trace element enrichment and the fact that these enrichments are indeed found in oceanic gabbros together indicate that upward reactive flow of interstitial melt in crystal mushes is a generic process that is expected to operate in any magma chamber in a mushy state. This is further supported by the fact that RPF is common in layered intrusions (Irvine, 1980; Bédard *et al.*, 1988; McBirney & Sonnenthal, 1990; Mathez, 1995; Boudreau, 1999; Namur *et al.*, 2013; Leuthold *et al.*, 2014). Hence, RPF appears to be the norm, not the exception, in mushy magma chambers.

The compositions of reactive melts

The available data enable us to place some constraints on the compositions of the melts responsible for the observed reactions. In some samples [e.g. the primitive olivine gabbro from Hess Deep (Fig. 3) and the 735B troctolite–olivine gabbro (Fig. 8a and b)], the reaction

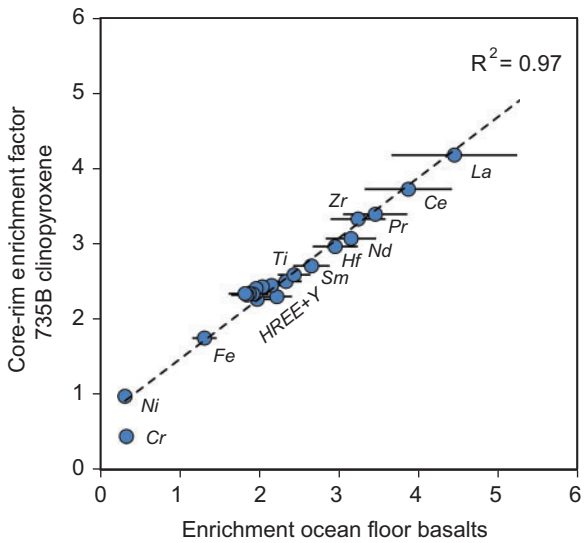

Fig. 11. Relationship between the trace element enrichment in MORB as determined from regressions of global trace element data (O'Neill & Jenner, 2012) and the enrichment observed in a clinopyroxene crystal from ODP Hole 735B. Enrichment in MORB is calculated for the window in which the replenishment model reaches steady state (8·6–5·6 wt% MgO) using the equations of O'Neill & Jenner (2012), with error bars representing the quoted uncertainties on the regressions. The high degree of correlation suggests a link between RPF in the lower oceanic crust and MORB; it should be noted that the absolute values do not necessarily have to correspond, as they are simply a function of the chosen MgO window of the MORB data and the degree of evolution of the studied crystal.

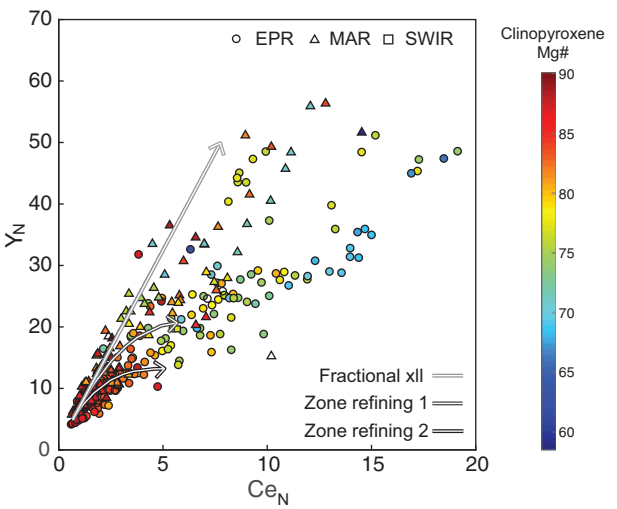

Fig. 12. Global compilation of chondrite-normalized (N) Ce vs Y in clinopyroxene from oceanic gabbros, with data points color-coded for clinopyroxene Mg#. Fractional crystallization pathway of clinopyroxene in equilibrium with MORB is as in Fig. 10, with a starting composition of $Ce_N = 0{\cdot}66$ and $Y_N = 4{\cdot}9$. Two zone refining models are shown, which were calculated using equation (1), using a cotectic assemblage (model 1) and an assemblage of 80% clinopyroxene–20% plagioclase (model 2). It should be noted that the global array shows over-enrichment of Ce relative to Y compared with fractional crystallization, and that this holds true for samples from the three main ocean basins (EPR, East Pacific Rise; MAR, Mid-Atlantic Ridge; SWIR, Southwest Indian Ridge). Zone refining can generate the observed Ce over-enrichment, with additional fractional crystallization of the resulting melts required to reproduce the evolved end of the global data array. Data are from Coogan *et al.* (2000, 2002*a*), Gao *et al.* (2007), Drouin *et al.* (2009) and Lissenberg *et al.* (2013).

products are olivine, plagioclase and clinopyroxene, suggesting that the reactive melts were relatively high-temperature, cotectic melts. Because their Mg# may have been buffered by reaction with the matrix (Lissenberg & Dick, 2008), using clinopyroxene Mg# or Fo contents of olivine as a tracer of the degree of evolution of these melts is problematic. Plagioclase anorthite contents are more reliable in this respect, because buffering is unlikely owing to the slow coupled NaSi–CaAl diffusion (Morse, 1984), although the reaction may modify the composition of the plagioclase in equilibrium with the reactive melt to some degree (Lissenberg & Dick, 2008). Plagioclase in the element maps of the primitive olivine gabbro from Hess Deep (Fig. 3) shows only minor zoning, with many rims maintaining An contents similar to the cores (An_{79}), indicating crystallization from primitive melts. Although still on the three-phase olivine–plagioclase–clinopyroxene cotectic, plagioclase in the olivine gabbro channel in the 735B troctolite–olivine gabbro, as well as the gabbro channel in the Kane troctolite (Lissenberg & Dick, 2008), has lower An contents (An_{54} and An_{67}, respectively), indicating that the reactive melts became more evolved. To investigate just how much more evolved these melts were, we ran a fractional crystallization model for the primary melt of Dick *et al.* (2000) using MELTS (Ghiorso & Sack, 1995), assuming 0·15% H_2O, oxygen fugacity of QFM – 1 and a pressure of 2 kbar. This primary melt composition was derived for the Southwest Indian Ridge; however, because its Na_2O contents are at the lower end of the Southwest Indian Ridge array, and are typical of Atlantic MORB, this melt is a reasonable approximation for both the Southwest Indian Ridge and Mid-Atlantic Ridge samples. The results are shown in Fig. 13, and indicate that melts crystallizing An_{67} (Kane) are basaltic, with an Mg# of ~56 (i.e. they are typical MORB). The An_{54} in the 735B olivine gabbro channel would have formed from more evolved MORB (Mg# ~40). Plagioclase extends to still lower An contents in some samples, indicating that reactive melts can reach highly evolved compositions (see below).

TiO_2 may be the best indicator of melt evolution in clinopyroxene, provided that the melt has not yet reached Fe–Ti oxide saturation; it is not a major constituent in olivine, plagioclase and clinopyroxene, and, being moderately (rather than highly) incompatible, is not very sensitive to the incompatible trace element over-enrichment induced by RPF. Figure 4 shows that the group of high-Cr clinopyroxenes that we attribute to reactions of melts with a primitive gabbroic matrix have TiO_2 contents of 0·3–1·1 wt %, indicating that these crystals formed from melts with ~0·7–2·4 wt % TiO_2 [for $D = 0{\cdot}45$, calculated from equation (606) of (Bédard, 2014) using typical oceanic clinopyroxene compositions]. The clinopyroxene in the 735B olivine gabbro channel (Fig. 8b) falls within this range as well, with a clinopyroxene TiO_2 of 0·86% indicating crystallization from a MORB melt with ~1·9% TiO_2. The global correlation between TiO_2 and Mg# in MORB indicates that the lower end of this TiO_2 range is typical for primitive MORB, with the higher end reflecting evolved MORB (Mg# < 50).

There are several observations that indicate that reactive melts can extend to highly evolved compositions: (1) evidence for saturation in trace phases; this evidence comes directly from petrographic and element map observations (e.g. the common occurrence of accessory apatite and zircon, as well as quartz, in the upper, most reacted parts of the Hess Deep section and the abundance of Fe–Ti oxides and apatite in Fig. 8d), and from clinopyroxene trace element data, which show decreasing Ti, P and Zr towards the rim in some crystals, reflecting saturation of Fe–Ti oxides, apatite and zircon, respectively; (2) the low An content of plagioclase in some reacted domains (e.g. An_{25} in the oxide gabbro of Fig. 8d); (3) the common association of reacted domains with brown amphibole (e.g. Fig. 2), indicating significant fractionation of MORB to reach elevated water activities. The fractional crystallization model for slow-spreading MORB compositions (Fig. 13) indicates that apatite saturates with ~12% melt mass remaining, when the melt has reached an Mg# of ~19, and is andesitic (SiO_2 ~ 60%). This provides a minimum degree of differentiation for the reactive melt forming the apatite-rich oxide gabbro in Fig. 8d. Its An_{25} plagioclase indicates the melt was in fact even more evolved (dacitic, with SiO_2 ~ 67%; Fig. 13).

In summary, the data indicate that reactive melts range in composition from primitive (basalts) to highly evolved (dacites), which implies that RPF occurs over the full temperature spectrum of evolution of oceanic plutonic rocks.

Testing competing models for MORB evolution

There are currently four competing hypotheses for the differentiation process of MORB: (1) fractional crystallization, which is the traditional model for MORB

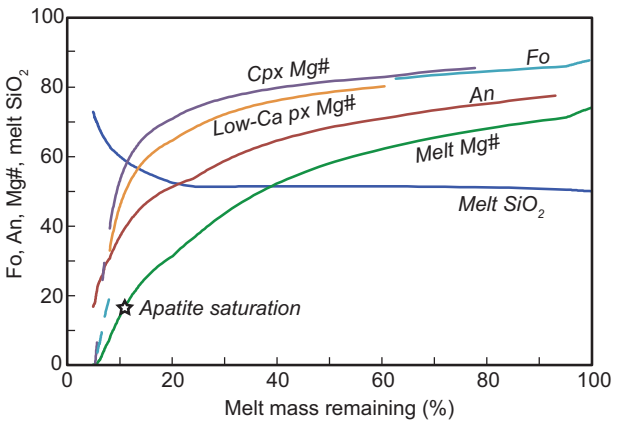

Fig. 13. Compositions of olivine, plagioclase, clinopyroxene, low-Ca pyroxene and melt as a function of melt mass remaining during differentiation of slow-spreading MORB. Primary melt composition was taken from Dick *et al.* (2000), and was modelled using MELTS (Ghiorso & Sack, 1995) at $P = 2$ kbar and QFM – 1. Star marks apatite saturation.

evolution, and relies on the instantaneous separation of saturated phases from the melt; owing to extensive phase equilibia studies, this can be predicted with reasonable accuracy (e.g. Grove *et al.*, 1992); (2) RepTapFrac, which describes a magma chamber that goes though cycles of replenishment (Rep) followed by melt extraction (Tap) and then fractional crystallization (Frac) (O'Hara, 1977; Albarède, 1985; O'Neill & Jenner, 2012); (3) *in situ* crystallization in a replenished magma chamber, during which a fractionating magma reservoir receives a contribution of enriched melt extracted from the underlying crystal mush (Langmuir, 1989; Coogan & O'Hara, 2015); (4) RPF, which posits that MORB includes a component of melts that evolved through reaction within a crystal mush (Lissenberg *et al.*, 2013). Contamination by assimilated hydrothermally altered crustal rocks (Coogan *et al.*, 2003; Wanless *et al.*, 2010), or partial melts thereof (France *et al.*, 2014), may add to the complexity, and appears to be particularly relevant for dacitic lavas (Wanless *et al.*, 2010).

Any successful model for the evolution of MORB needs to fulfil three criteria: (1) it needs to reproduce the compositional array of MORB; (2) it needs to be consistent with the rock record; (3) it needs to be compatible with available constraints on the nature of mid-ocean ridge magma chambers. The first of these criteria only partly discriminates between the four models for MORB evolution. As shown previously, fractional crystallization cannot reproduce the trace element distribution patterns of MORB (Bryan & Moore, 1977; White & Bryan, 1977; Dungan & Rhodes, 1978; O'Neill & Jenner, 2012; Lissenberg *et al.*, 2013), and thus fails the first test. RepTapFrac and *in situ* crystallization can both successfully reproduce the MORB trace elements (O'Neill & Jenner, 2012; Coogan & O'Hara, 2015), and we have shown in this study that the same is true for RPF (Fig. 11).

The second of the three criteria is that the proposed mechanism is compatible with the rock record. As outlined above, this is not the case for fractional crystallization: it requires a high proportion of mineral fractionation at high pressures, which is not compatible with existing constraints on the crystallization depths of plutonic rocks, and cannot reproduce the trace element distributions in the gabbroic rocks. Only RPF can account for the depletion in clinopyroxene cores, plagioclase and olivine: in fractional crystallization, RepTapFrac and *in situ* crystallization models, crystallization is governed by equilibrium partitioning at the crystal–melt interface during crystal growth, which would prevent the formation of highly depleted crystals from melts with MORB compositions. This does not, however, rule out RepTapFrac and *in situ* crystallization models, as RPF could, in principle, represent an overprint on cumulates produced in RepTapFrac or *in situ* magma chambers, although the fact that reactions are also found in gabbroic xenoliths in axial lavas (Gurenko & Sobolev, 2006; Ridley *et al.*, 2006) indicates that reactions occur at least in part beneath the ridge axis.

The third criterion is that the model needs to be compatible with the constraints on the nature of mid-ocean ridge magma chambers, which we briefly review here. At the magmatically most robust spreading ridges such as the East Pacific Rise, seismic data have identified a melt lens at the base of the sheeted dykes, which is present along much of the ridge axis (Harding *et al.*, 1989; Kent *et al.*, 1990, 1993; Vera *et al.*, 1990; Carbotte *et al.*, 2013). An important, but generally neglected, observation is that the melt lens is composed of crystal mush (<40% melt) along substantial proportions of its length (80–90% at 14°S, >75% at 9°N), with only 2–4 km sections containing high (>70%) melt fractions (Singh *et al.*, 1998; Xu *et al.*, 2014). This kilometre-scale petrological segmentation is superimposed on small-scale (hundreds of metres) variations in crystal content (Marjanović *et al.*, 2015). The variation in crystallinity is most probably the result of the very short time scales (a few decades) of cooling of melt to mush in an axial melt lens (Singh *et al.*, 1998). The melt lens overlies a large region characterized by low seismic velocities interpreted as a crystal mush with a small (<15%) average proportion of melt (Crawford *et al.*, 1999; Vera *et al.*, 1990; Dunn *et al.*, 2000; Crawford & Webb, 2002), which contains sills with higher melt fractions (Canales *et al.*, 2009; Marjanovic *et al.*, 2014).

At slow-spreading ridges (away from hotspots) the magmatic system is less robust, and melt-rich bodies are scarce (Detrick *et al.*, 1990), with the Lucky Strike segment the only segment documented to date with an axial melt lens (Singh *et al.*, 2006; Combier *et al.*, 2015). It overlies a lower crustal low-velocity zone that may contain a small (1%) portion of melt (Seher *et al.*, 2010). Along the rest of the Mid-Atlantic Ridge, no melt-rich bodies have been found: where present, melts occur in small proportions (most probably a few per cent) in low-velocity zones occupying the deeper (2–10 km) parts of the crust and uppermost mantle (Canales *et al.*, 2000; Dunn *et al.*, 2005). The scarcity of magma-rich bodies at slow-spreading ridges is consistent with microearthquakes generally extending to 5–8 km (Toomey *et al.*, 1985; Kong *et al.*, 1992; Wolfe *et al.*, 1995; Barclay *et al.*, 2001), indicating that the crust is characterized by a relatively cool thermal structure (Dusunur *et al.*, 2009). It is also consistent with ridge axis thermal models (Sleep, 1975; Chen, 2004). Together, a picture emerges of a relatively cool ridge axis with episodic emplacement of melts, which then cool quickly to a mush before complete solidification. It is these constraints that models for MORB evolution must take into account.

One of the main distinguishing features between the RPF model on the one hand, and the RepTapFrac and *in situ* models on the other, is the nature of the magma chamber. RPF requires a crystal mush to operate, whereas RepTapFrac and the *in situ* crystallization model require a long-lived and melt-filled magma chamber. The RepTapFrac parameterization indicates that as many as several hundred cycles are required to

explain the abundances of incompatible trace elements such as La at 5·6% MgO (the limit of the steady-state operation of RepTapFrac; O'Neill & Jenner, 2012) The *in situ* crystallization of Coogan & O'Hara (2015) is proposed to occur in similarly replenished magma chambers. As discussed above, the geophysical constraints indicate that crystal mush is the norm in oceanic magma chambers, and that melt turns into mush quickly. This is true even for the melt lens at fast-spreading ridges; at slow-spreading ridges, there is a near absence of melt-filled magma chambers. These constraints pose a serious challenge to models that depend on the presence of long-lived, melt-rich magma chambers. In contrast, the common occurrence of crystal mush provides favourable conditions for RPF to operate. Because the over-enrichment is observed in lavas across the spreading rate spectrum, but long-lived melt-rich magma chambers apparently are not, we argue that RPF is the most viable mechanism to explain the MORB array.

SYNTHESIS AND OUTLOOK

The data presented here demonstrate that RPF is a common—if not ubiquitous—process in oceanic magma chambers. It changes both major and trace elements in the crystal mush, and leads to the formation of melts with compositions that do not match conventional crystallization models. Both the occurrence of RPF and the resulting changes in melt composition are predictable consequences of the mushy state of magma chambers (Solano *et al.*, 2014), and similar features are also present in layered intrusions on the continents (e.g. Irvine, 1980). Together, this suggests that reactive porous flow is intrinsic to large mafic magma chambers.

The apparent ubiquity of RPF in mid-ocean ridge magma chambers, coupled with the excellent fit between the trace element distributions caused by RPF and those observed in ocean floor basalts (Fig. 11), leads us to posit that RPF has a major control on the evolution of MORB. We contend that if the trace element evolution in the plutonic rocks matches that in the volcanic rocks, the likelihood is that the same process is responsible for both. It would be highly fortuitous if the trace element distributions in erupted lavas matched those in their crystal residues but they result from different processes. RPF can account not only for the observed trace element over-enrichment in plutonic and volcanic rocks, but also the apparent high-pressure signal in both MORB (shifts in $MgO–CaO–Al_2O_3$) and gabbroic rocks (high-Mg# clinopyroxene). Our model for the evolution of MORB is thus a holistic one, tying together the evolution of the plutonic and volcanic components of the system.

We envisage the following general scenario for MORB evolution. Primary melts are emplaced as melt-rich bodies in the lower crustal crystal mush (fast-spreading ridges and magmatically robust slow-spreading ridge segments) or in already cooled lower crust or upper mantle (magma-poor slow- and ultraslow-spreading ridge segments). The high crystallization rate over a limited temperature interval after plagioclase saturation (Kelemen & Aharonov, 1998) rapidly leads to the formation of a crystal framework. Owing to the buoyancy of the interstitial melt the mush compacts, leading to melt migration by porous flow and the associated reactions described here. Because porous flow leads to the formation of melt-rich layers in the crystal mush (Solano *et al.*, 2014), melts with an RPF signature (over-enriched trace elements and/or modified $MgO–CaO–Al_2O_3$) are extracted from the crystal mush and concentrated. This facilitates upward transport of these melts, either to feed eruptions, or to feed into melt-rich bodies further up-section. In addition, the crustal-scale over-enrichment in trace elements (Fig. 9) indicates that there is a pervasive low-volume flux of reactive melt, which may mix into eruptible reservoirs (Lissenberg *et al.*, 2013). The end product is a plutonic section and overlying volcanic rocks that both carry the distinct signature of RPF.

Our understanding of the RPF process is only in its infancy. A number of different approaches would improve this. One of these is experimental studies, which would allow reconstruction of the rates, mechanisms and chemical consequences of melt–crystal reaction (e.g. Kvassnes & Grove, 2008; Leuthold *et al.*, 2015). Physico-chemical models have the potential to shed further light on the conditions required for RPF, the percolation rates and potential length scales involved, the extraction mechanisms of melts from crystal mushes, and, if phase diagrams are included (see Solano *et al.*, 2014), the chemical consequences of RPF. Stable isotope constraints (e.g. Pogge von Strandmann *et al.*, 2015) have the potential to provide information on the time scales involved. Finally, the rock record can be mined to build up a database of relevant observations, which serve as a benchmark for the experimental and modelling studies. In particular, the detailed study of samples taken from a well-defined field context has the potential to add significantly to our understanding of RPF.

FUNDING

This work was supported by the Natural Environment Research Council NERC Grant NE/I001670/1 to C.J.L. and used samples and/or data provided by the Ocean Drilling Program (ODP). ODP is sponsored by the US National Science Foundation (NSF) and participating countries under management of Joint Oceanographic Institutions (JOI), Inc.

SUPPLEMENTARY DATA

Supplementary data for this paper are available at *Journal of Petrology* online.

ACKNOWLEDGEMENTS

C.J.L. thanks Jean Bédard for introducing him to the world of melt–rock reaction, and Henry Dick for fostering this and for sharing his insights into the evolution of ODP Hole 735B. Andy Milton is thanked for assistance with the LA-ICP-MS analyses. The assistance of the staff at the Kochi core repository is gratefully acknowledged.

REFERENCES

Albarède, F. (1985). Regime and trace-element evolution of open magma chambers. *Nature* **318**, 356–358.

Anders, E. & Grevesse, N. (1989). Abundances of the elements: Meteoritic and solar. *Geochimica et Cosmochimica Acta* **53**, 197–214.

Baines, A. G., Cheadle, M. J., Dick, H. J. B., Scheirer, A. H., John, B. E., Kusznir, N. J. & Matsumoto, T. (2007). Evolution of the Southwest Indian Ridge from 55°45′E to 62°E: Changes in plate-boundary geometry since 26 Ma. *Geochemistry, Geophysics, Geosystems* **8**, doi:10.1029/2006GC001559.

Barclay, A. H., Toomey, D. R. & Solomon, S. C. (2001). Microearthquake characteristics and crustal V_P/V_S structure at the Mid-Atlantic Ridge, 35°N. *Journal of Geophysical Research: Solid Earth* **106**, 2017–2034.

Beard, J. S., Ragland, P. C. & Rushmer, T. (2004). Hydration crystallization reactions between anhydrous minerals and hydrous melt to yield amphibole and biotite in igneous rocks: description and implications. *Journal of Geology* **112**, 617–621.

Bédard, J. (2001). Parental magmas of the Nain Plutonic Suite anorthosites and mafic cumulates: a trace element modelling approach. *Contributions to Mineralogy and Petrology* **141**, 747–771.

Bédard, J. H. (1991). Cumulate recycling and crustal evolution in the Bay of Islands ophiolite. *Journal of Geology* **99**, 225–249.

Bédard, J. H. (2014). Parameterizations of calcic clinopyroxene—Melt trace element partition coefficients. *Geochemistry, Geophysics, Geosystems* **15**, 303–336.

Bédard, J. H., Sparks, R. S. J., Renner, R., Cheadle, M. J. & Hallworth, M. A. (1988). Peridotite sills and metasomatic gabbros in the Eastern Layered Series of the Rhum complex. *Journal of the Geological Society, London* **145**, 207–224.

Bédard, J. H., Hebert, R., Berclaz, A. & Varfalvy, V. (2000). Syntexis and the genesis of lower oceanic crust. In: Dilek, Y., Moores, E. M., Elthon, D. & Nicolas, A. (eds) *Ophiolites and Oceanic Crust: New Insights from Field Studies and the Ocean Drilling Program. Geological Society of America, Special Papers* **349**, 105–119.

Blackman, D. K., Ildefonse, B., John, B. E., Ohara, Y., Miller, D. J., MacLeod, C. J. & Expedition 304/305 Scientists (2006). *Proceedings of the Integrated Ocean Drilling Program, 304/305*. Integrated Ocean Drilling Program, College Station TX.

Boudier, F., Nicolas, A. & Ildefonse, B. (1996). Magma chambers in the Oman ophiolite: fed from the top and the bottom. *Earth and Planetary Science Letters* **144**, 239–250.

Boudreau, A. (1999). Fluid fluxing of cumulates: the J-M Reef and associated rocks of the Stillwater Complex, Montana. *Journal of Petrology* **40**, 755–772.

Bryan, W. B. & Moore, J. G. (1977). Compositional variations of young basalts in the Mid-Atlantic Ridge rift valley near lat 36°49′N. *Geological Society of America Bulletin* **88**, 556–570.

Canales, J. P., Collins, J. A., Escartin, J. & Detrick, R. S. (2000). Seismic structure across the rift valley of the Mid-Atlantic Ridge at 23°20′ (MARK area); implications for crustal accretion processes at slow spreading ridges. *Journal of Geophysical Research, B, Solid Earth* **105**, 28411–28425.

Canales, J. P., Nedimovic, M. R., Kent, G. M., Carbotte, S. M. & Detrick, R. S. (2009). Seismic reflection images of a near-axis melt sill within the lower crust at the Juan de Fuca ridge. *Nature* **460**, 89–93.

Carbotte, S. M., Marjanovic, M., Carton, H., Mutter, J. C., Canales, J. P., Nedimovic, M. R., Han, S. & Perfit, M. R. (2013). Fine-scale segmentation of the crustal magma reservoir beneath the East Pacific Rise. *Nature Geoscience* **6**, 866–870.

Chakraborty, S. (1997). Rates and mechanisms of Fe–Mg interdiffusion in olivine at 980°–1300°. *Journal of Geophysical Research* **102**, 12317–12331.

Chen, Y. J. (2004). Modeling the thermal state of the oceanic crust. In: German, C. R., Lin, J. & Parson, L. M. (eds) *Mid-Ocean Ridges: Hydrothermal Interactions Between the Lithosphere and Oceans. American Geophysical Union, Geophysical Monograph* **148**, 95–110.

Combier, V., Seher, T., Singh, S. C., Crawford, W. C., Cannat, M., Escartín, J. & Dusunur, D. (2015). Three-dimensional geometry of axial magma chamber roof and faults at Lucky Strike volcano on the Mid-Atlantic Ridge. *Journal of Geophysical Research: Solid Earth* **120**, 5379–5400.

Coogan, L. A. (2014). The lower oceanic crust. In: Turekian, K. K. & Holland, H. D. (eds) *Treatise on Geochemistry*, 2nd edn. Elsevier, pp. 497–541.

Coogan, L. A. & O'Hara, M. J. (2015). MORB differentiation: *In situ* crystallization in replenished–tapped magma chambers. *Geochimica et Cosmochimica Acta* **158**, 147–161.

Coogan, L. A., Saunders, A. D., Kempton, P. D. & Norry, M. J. (2000). Evidence from oceanic gabbros for porous melt migration within a crystal mush beneath the Mid-Atlantic Ridge. *Geochemistry, Geophysics, Geosystems* **1**, doi:10.1029/2000GC000072.

Coogan, L. A., Wilson, R. N., Gillis, K. M. & MacLeod, C. J. (2001). Near-solidus evolution of oceanic gabbros: insights from amphibole geochemistry. *Geochimica et Cosmochimica Acta* **65**, 4339–4357.

Coogan, L. A., Gillis, K. M., MacLeod, C. J., Thompson, G. M. & Hékinian, R. (2002a). Petrology and geochemistry of the lower ocean crust formed at the East Pacific Rise and exposed at Hess Deep: A synthesis and new results. *Geochemisty, Geophysics, Geosystems* **3**, doi:10.1029/2001GC000230.

Coogan, L. A., Thompson, G. & MacLeod, C. J. (2002b). A textural and geochemical investigation of high level gabbros from the Oman Ophiolite; implications for the role of the axial magma chamber at fast-spreading ridges. *Lithos* **63**, 67–82.

Coogan, L. A., Mitchell, N. C. & O'Hara, M. J. (2003). Roof assimilation at fast spreading ridges; an investigation combining geophysical, geochemical, and field evidence. *Journal of Geophysical Research, B, Solid Earth* **108**, doi:10.1029/2001JB001171.

Coogan, L. A., Jenkin, G. R. T. & Wilson, R. N. (2007). Contrasting cooling rates in the lower oceanic crust at fast- and slow-spreading ridges revealed by geospeedometry. *Journal of Petrology* **48**, 2211–2231.

Crawford, W. C. & Webb, S. C. (2002). Variations in the distribution of magma in the lower crust and at the Moho beneath the East Pacific Rise at 9°–10°N. *Earth and Planetary Science Letters* **203**, 117–130.

Crawford, W. C., Webb, S. C. & Hildebrand, J. A. (1999). Constraints on melt in the lower crustal and Moho at the East Pacific Rise, 9°48′N, using seafloor compliance

measurements. *Journal of Geophysical Research, B, Solid Earth* **104**, 2923–2939.

Danyushevsky, L. V., Sobolev, A. V. & Dmitriev, L. V. (1996). Estimation of the pressure of crystallization and H_2O content of MORB and BABB glasses: calibration of an empirical technique. *Mineralogy and Petrology* **57**, 185–204.

Danyushevsky, L. V., Perfit, M. R., Eggins, S. M. & Falloon, T. J. (2003). Crustal origin for coupled 'ultra-depleted' and 'plagioclase' signatures in MORB olivine-hosted melt inclusions: evidence form the Siqueiros Transform Fault, East Pacific Rise. *Contributions to Mineralogy and Petrology* **144**, 619–637.

Detrick, R. S., Mutter, J. C., Buhl, P. & Kim, I. I. (1990). No evidence from multichannel reflection data for a crustal magma chamber in the MARK area on the Mid-Atlantic Ridge. *Nature* **347**, 61–64.

Dick, H. J. B., Natland, J. H., Alt, J. C., et al. (2000). A long *in-situ* section of the lower ocean crust: results of ODP Leg 176 drilling at the Southwest Indian Ridge. *Earth and Planetary Science Letters* **179**, 31–51.

Dick, H. J. B., Ozawa, K., Meyer, P. S., Niu, Y., Robinson, P. T., Constantin, M., Hebert, R., Maeda, J., Natland, J. H., Hirth, G. & Mackie, S. (2002). Primary silicate mineral chemistry of a 1·5-km section of very slow spreading lower ocean crust: ODP Hole 735B, Southwest Indian Ridge. In: Natland, J. H., Dick, H. J. B., Miller, D. J. & Von Herzen, R. (eds) *Proceedings of the Ocean Drilling Program, Scientific Results*. Ocean Drilling Program **176**, 1–60. [CD-ROM].

Dick, H. J. B., Lin, J. & Schouten, H. (2003). An ultraslow-spreading class of ocean ridge. *Nature* **426**, 405–412.

Dick, H. J. B., Tivey, M. A. & Tucholke, B. E. (2008). Plutonic foundation of a slow-spread ridge segment: the oceanic core complex at Kane Megamullion, 23°30′N, 45°20′W. *Geochemistry, Geophysics, Geosystems*, doi:10.1029/2007GC001645.

Dimanov, A. & Wiedenbeck, M. (2006). (Fe,Mn)–Mg interdiffusion in natural diopside: effect of pO_2. *European Journal of Mineralogy* **18**, 705–718.

Drouin, M., Godard, M., Ildefonse, B., Bruguier, O. & Garrido, C. J. (2009). Geochemical and petrographic evidence for magmatic impregnation in the oceanic lithosphere at Atlantis Massif, Mid-Atlantic Ridge (IODP Hole U1309D, 30°N). *Chemical Geology* **264**, 71–88.

Drouin, M., Ildefonse, B. & Godard, M. (2010). A microstructural imprint of melt impregnation in slow spreading lithosphere: Olivine-rich troctolites from the Atlantis Massif, Mid-Atlantic Ridge, 30°N, IODP Hole U1309D. *Geochemistry, Geophysics, Geosystems* **11**, Q06003.

Dungan, M. A. & Rhodes, J. M. (1978). Residual glasses and melt inclusions in basalts from DSDP Legs 45 and 46: evidence for magma mixing. *Contributions to Mineralogy and Petrology* **67**, 417–431.

Dunn, R. A., Toomey, D. R. & Solomon, S. C. (2000). Three-dimensional seismic structure and physical properties of the crust and shallow mantle beneath the East Pacific Rise at 9°30′N. *Journal of Geophysical Research* **105**, 23537–23555.

Dunn, R. A., Lekic, V., Detrick, R. S. & Toomey, D. R. (2005). Three-dimensional seismic structure of the Mid-Atlantic Ridge (35°N): Evidence for focused melt supply and lower crustal dike injection. *Journal of Geophysical Research* **110**, doi:10.1029/2004JB003473.

Dusunur, D., Escartín, J., Combier, V., Seher, T., Crawford, W., Cannat, M., Singh, S. C., Matias, L. M. & Miranda, J. M. (2009). Seismological constraints on the thermal structure along the Lucky Strike segment (Mid-Atlantic Ridge) and interaction of tectonic and magmatic processes around the magma chamber. *Marine Geophysical Researches* **30**, 105–120.

Eason, D. E. & Sinton, J. M. (2009). Lava shields and fissure eruptions of the Western Volcanic Zone, Iceland: Evidence for magma chambers and crustal interaction. *Journal of Volcanology and Geothermal Research* **186**, 331–348.

Elthon, D., Stewart, M. & Ross, K. (1992). Compositional trends of minerals in oceanic cumulates. *Journal of Geophysical Research* **97**, 15189–15199.

France, L., Koepke, J., MacLeod, C. J., Ildefonse, B., Godard, M. & Deloule, E. (2014). Contamination of MORB by anatexis of magma chamber roof rocks: Constraints from a geochemical study of experimental melts and associated residues. *Lithos* **202–203**, 120–137.

Francheteau, J., Armiho, R., Cheminee, J. L., Hekinian, R., Lonsdale, P. & Blumm, N. (1990). 1 Ma East Pacific Rise oceanic crust and uppermost mantle exposed by rifting in Hess Deep (equatorial Pacific Ocean). *Earth and Planetary Science Letters* **101**, 281–295.

Gao, Y., Hoefs, J., Hellebrand, E., von der Handt, A. & Snow, J. (2007). Trace element zoning in pyroxenes from ODP Hole 735B gabbros: diffusive exchange or synkinematic crystal fractionation?. *Contributions to Mineralogy and Petrology* **153**, 429–442.

Ghiorso, M. S. & Sack, R. O. (1995). Chemical mass transfer in magmatic processes IV. A revised and internally consistent thermodynamic model for the interpolation and extrapolation of liquid–solid equilibria in magmatic systems at elevated temperatures and pressures. *Contributions to Mineralogy and Petrology* **119**, 197–212.

Gillis, K. M., Snow, J. E., Klaus, A., et al. (2014). Primitive layered gabbros from fast-spreading lower oceanic crust. *Nature* **505**, 204–207.

Godard, M., Bosch, D. & Einaudi, F. (2006). A MORB source for low-Ti magmatism in the Semail ophiolite. *Chemical Geology* **234**, 58–78.

Grimes, C. B., Cheadle, M. J., John, B. E., Reiners, P. W. & Wooden, J. L. (2011). Cooling rates and the depth of detachment faulting at oceanic core complexes: Evidence from zircon Pb/U and (U–Th)/He ages. *Geochemistry, Geophysics, Geosystems* **12**, Q0AG01.

Grove, T. L. & Bryan, W. B. (1983). Fractionation of pyroxene-phyric MORB at low pressure: An experimental study. *Contributions to Mineralogy and Petrology* **84**, 293–309.

Grove, T. L., Kinzler, R. J. & Bryan, W. B. (1990). Natural and expirimental phase relations of lavas from Serocki volcano. In: Detrick, R., Honnorez, J., Bryan, W. B., et al (eds) *Proceedings of the Ocean Drilling Program, Scientific Results, 106/109*. Ocean Drilling Program, College Station TX, pp. 9–16.

Grove, T. L., Kinzler, R. J. & Bryan, W. B. (1992). Fractionation of mid-ocean ridge basalt (MORB). In: Phipps Morgan, J., Blackman, D. K. & Sinton, J. M. (eds) *Mantle Flow and Melt Generation at Mid-Ocean Ridges. American Geophysical Union, Geophysical Monograph* **71**, 281–310.

Gurenko, A. & Sobolev, A. (2006). Crust–primitive magma interaction beneath neovolcanic rift zone of Iceland recorded in gabbro xenoliths from Midfell, SW Iceland. *Contributions to Mineralogy and Petrology* **151**, 495–520.

Harding, A. J., Orcutt, J. A., Kappus, M. E., Vera, E. E., Mutter, J. C., Buhl, P., Detrick, R. S. & Brocher, T. M. (1989). Structure of young oceanic crust at 13°N on the East Pacific Rise from expanding spread profiles. *Journal of Geophysical Research, B: Solid Earth* **94**, 12163–12196.

Harris, P. G. (1957). Zone refining and the origin of potassic basalts. *Geochimica et Cosmochimica Acta* **12**, 195–208.

Herzberg, C. (2004). Partial crystallization of mid-ocean ridge basalts in the crust and mantle. *Journal of Petrology* **45**, 2389–2405.

Huber, C., Bachmann, O. & Dufek, J. (2011). Thermo-mechanical reactivation of locked crystal mushes: Melting-induced internal fracturing and assimilation processes in magmas. *Earth and Planetary Science Letters* **304**, 443–454.

Irvine, T. (1980). Magmatic infiltration metasomatism, double-diffusive fractional crystallization, and adcumulus growth in the Muskox intrusion and other layered intrusions. In: Hargraves, R. B. (ed.) *Physics of Magmatic Processes*. Princeton University Press, pp. 325–383.

Kamenetsky, V. & Gurenko, A. (2007). Cryptic crustal contamination of MORB primitive melts recorded in olivine-hosted glass and mineral inclusions. *Contributions to Mineralogy and Petrology* **153**, 465–481.

Kelemen, P. B. & Aharonov, E. (1998). Periodic formation of magma fractures and generation of layered gabbros in the lower crust beneath oceanic spreading ridges. In: Buck, W., Delaney, P. T., Karson, J. A. & Lagabrielle, Y. (eds) *Faulting and Magmatism at Mid-Ocean Ridges. American Geophysical Union, Geophysical Monograph* **106**, 267–290.

Kelemen, P. B., Kikawa, E., Miller, D. J., et al. (2004). *Proceedings of the Ocean Drilling Program, Initial Reports 209*. Ocean Drilling Program, College Station TX.

Kent, G. M., Harding, A. J. & Orcutt, J. A. (1990). Evidence for a smaller magma chamber beneath the East Pacific Rise at 9°30′N. *Nature* **344**, 650–653.

Kent, G. M., Harding, A. J. & Orcutt, J. A. (1993). Distribution of magma beneath the East Pacific Rise between the Clipperton Transform and the 9°17′N Deval from forward modeling of common depth point data. *Journal of Geophysical Research, B: Solid Earth* **98**, 13945–13969.

Klein, E. M. & Langmuir, C. H. (1987). Global correlations of ocean ridge basalt chemistry with axial depth and crustal thickness. *Journal of Geophysical Research* **92**, 8089–8115.

Kong, L. S. L., Solomon, S. C. & Purdy, G. M. (1992). Microearthquake characteristics of a mid-ocean ridge along-axis high. *Journal of Geophysical Research* **97**, 1659–1685.

Kvassnes, A. & Grove, T. (2008). How partial melts of mafic lower crust affect ascending magmas at oceanic ridges. *Contributions to Mineralogy and Petrology* **156**, 49–71.

Langmuir, C. H. (1989). Geochemical consequences of *in situ* crystallization. *Nature* **340**, 199–205.

Langmuir, C. H., Klein, E. M. & Plank, T. (1992). Petrological systematics of mid-ocean ridge basalts: constraints on melt generation beneath ocean ridges. In: Phipps Morgan, J., Blackman, D. K. & Sinton, J. M. (eds) *Mantle Flow and Melt Generation at Mid-Ocean Ridges. American Geophysical Union, Geophysical Monograph* **71**, 183–280.

Laubier, M., Gale, A. & Langmuir, C. H. (2012). Melting and crustal processes at the FAMOUS segment (Mid-Atlantic Ridge): new insights from olivine-hosted melt inclusions from multiple samples. *Journal of Petrology* **53**, 665–698.

Lehnert, K., Su, Y., Langmuir, C. H., Sarbas, B. & Nohl, U. (2000). A global geochemical database structure for rocks. *Geochemistry, Geophysics, Geosystems* **1**, doi:10.1029/1999GC000026.

Leuthold, J., Blundy, J. D., Holness, M. B. & Sides, R. (2014). Successive episodes of reactive liquid flow through a layered intrusion (Unit 9, Rum Eastern Layered Intrusion, Scotland). *Contributions to Mineralogy and Petrology* **168**, doi:10.1007/s00410-014-1021-7.

Leuthold, J., Blundy, J. D. & Brooker, R. A. (2015). Experimental petrology constraints on the recycling of mafic cumulate: a focus on Cr-spinel from the Rum Eastern Layered Intrusion, Scotland. *Contributions to Mineralogy and Petrology* **170**, doi:10.1007/s00410-015-1165-0.

Liang, Y. (2003). Kinetics of crystal–melt reaction in partially molten silicates: 1. Grain scale processes. *Geochemistry, Geophysics, Geosystems* **4**, 10.1029/2002GC000375.

Lissenberg, C. J. & Dick, H. J. B. (2008). Melt–rock reaction in the lower oceanic crust and its implications for the genesis of mid-ocean ridge basalt. *Earth and Planetary Science Letters* **271**, 311–325.

Lissenberg, C. J., MacLeod, C. J., Howard, K. A. & Godard, M. (2013). Pervasive reactive melt migration through fast-spreading lower oceanic crust (Hess Deep, equatorial Pacific Ocean). *Earth and Planetary Science Letters* **361**, 436–447.

Lissenberg, C. J., Rioux, M., MacLeod, C. J., Bowring, S. A. & Shimizu, N. (2016). Crystallization depth beneath an oceanic detachment fault (ODP Hole 923A, Mid-Atlantic Ridge). *Geochemistry, Geophysics, Geosystems* **17**, 162–180.

MacLeod, C. J. & Yaouancq, G. (2000). A fossil melt lens in the Oman Ophiolite; implications for magma chamber processes at fast spreading ridges. *Earth and Planetary Science Letters* **176**, 357–373.

MacLeod, C. J., Boudier, G., Yaouancq, G. & Richter, C. (1996). Gabbro fabrics from Site 894, Hess Deep: implications for magma chamber processes at the East Pacific Rise. In: Mevel, C., Gillis, K. M., Allan, J. F. & Meyer, P. S. (eds) *Proceedings of the Ocean Drilling Program, Scientific Results, 147*. Ocean Drilling Program, College Station TX, pp. 317–328.

MacLeod, C. J., Lissenberg, C. J. & Bibby, L. E. (2013). 'Moist MORB' axial magmatism in the Oman ophiolite: The evidence against a mid-ocean ridge origin. *Geology* **41**, 459–462.

Marjanovic, M., Carbotte, S. M., Carton, H., Nedimovic, M. R., Mutter, J. C. & Canales, J. P. (2014). A multi-sill magma plumbing system beneath the axis of the East Pacific Rise. *Nature Geoscience* **7**, 825–829.

Marjanović, M., Carton, H., Carbotte, S. M., Nedimović, M. R., Mutter, J. C. & Canales, J. P. (2015). Distribution of melt along the East Pacific Rise from 9°30′ to 10°N from an amplitude variation with angle of incidence (AVA) technique. *Geophysical Journal International* **203**, doi:10.1093/gji/ggv251.

Mathez, E. A. (1995). Magmatic metasomatism and formation of the Merensky reef, Bushveld Complex. *Contributions to Mineralogy and Petrology* **119**, 277–286.

McBirney, A. R. (1987). Constitutional zone refining of layered intrusions. In: Parsons, I. (ed.) *Origins of Igneous Layering*. D. Reidel, pp. 437–452.

McBirney, A. R. & Sonnenthal, E. L. (1990). Metasomatic replacement in the Skærgaard Intrusion, East Greenland: Preliminary observations. *Chemical Geology* **88**, 245–260.

Meyer, P. S., Dick, H. J. B. & Thompson, G. (1989). Cumulate gabbros from the Southwest Indian Ridge, 54°S, 7°16′E: implications for magmatic processes at a slow spreading ridge. *Contributions to Mineralogy and Petrology* **103**, 44–63.

Michael, P. J. & Cornell, W. C. (1998). Influence of spreading rate and magma supply on crystallization and assimilation beneath mid-ocean ridges: Evidence from chlorine and major element chemistry of mid-ocean ridge basalts. *Journal of Geophysical Research* **103**, 18325–18356.

Miller, D. J., Abratis, M., Christie, D., et al. (2009). Data report: microprobe analyses of primary mineral phases from Site U1309, Atlantis Massif, IODP Expedition 304/305. In: Blackman, D. K., Ildefonse, B., John, B. E., et al (eds) *Proceedings of IODP* 304/305, Integrated Ocean Drilling

Program Management International, doi:10.2204/iodp.proc.304305.202.2009.

Morse, S. A. (1984). Cation diffusion in plagioclase feldspar. *Science* **225**, 504–505.

Müller, T., Dohmen, R., Becker, H. W., ter Heege, J. & Chakraborty, S. (2013). Fe–Mg interdiffusion rates in clinopyroxene: experimental data and implications for Fe–Mg exchange geothermometers. *Contributions to Mineralogy and Petrology* **166**, 1563–1576.

Namur, O., Humphreys, M. C. S. & Holness, M. B. (2013). Lateral reactive infiltration in a vertical gabbroic crystal mush, Skaergaard Intrusion, East Greenland. *Journal of Petrology* **54**, 985–1016.

Natland, J. H. & Dick, H. J. B. (2001). Formation of the lower ocean crust and the crystallization of gabbroic cumulates at a very slow spreading ridge. *Journal of Volcanology and Geothermal Research* **110**, 191–233.

O'Hara, M. J. (1977). Geochemical evolution during fractional crystallisation of a periodically refilled magma chamber. *Nature* **266**, 503–507.

O'Neill, H. S. C. & Jenner, F. E. (2012). The global pattern of trace-element distributions in ocean floor basalts. *Nature* **491**, 698–704.

Pfann, W. G. (1952). Principles of zone-melting. *Transactions of AIME* **194**, 747–753.

Pogge von Strandmann, P. A. E., Dohmen, R., Marschall, H. R., Schumacher, J. C. & Elliott, T. (2015). Extreme magnesium isotope fractionation at outcrop scale records the mechanism and rate at which reaction fronts advance. *Journal of Petrology* **56**, 33–58.

Rhodes, J. M., Dungan, M. A., Blanchard, D. P. & Long, P. E. (1979). Magma mixing at mid-ocean ridges: evidence from basalts drilled near 22°N on the Mid-Atlantic Ridge. *Tectonophysics* **55**, 35–61.

Ridley, W. I., Perfit, M. R., Smith, M. C. & Fornari, D. J. (2006). Magmatic processes in developing oceanic crust revealed in a cumulate xenolith collected at the East Pacific Rise, 9°50°N. *Geochemistry, Geophysics, Geosystems* **7**, doi:10.1029/2006GC001316.

Rioux, M., Lissenberg, C. J., McLean, N., Bowring, S. A., MacLeod, C. J., Hellebrand, E. & Shimizu, N. (2012). Protracted timescales of lower crustal growth at the fast-spreading East Pacific Rise. *Nature Geoscience* **5**, 275–278.

Sanfilippo, A., Tribuzio, R. & Tiepolo, M. (2014). Mantle–crust interactions in the oceanic lithosphere: Constraints from minor and trace elements in olivine. *Geochimica et Cosmochimica Acta* **141**, 423–439.

Sanfilippo, A., Morishita, T., Kumagai, H., Nakamura, K., Okino, K., Hara, K., Tamura, A. & Arai, S. (2015a). Hybrid troctolites from mid-ocean ridges: inherited mantle in the lower crust. *Lithos* **232**, 124–130.

Sanfilippo, A., Tribuzio, R., Tiepolo, M. & Berno, D. (2015b). Reactive flow as dominant evolution process in the lowermost oceanic crust: evidence from olivine of the Pineto ophiolite (Corsica). *Contributions to Mineralogy and Petrology* **170**, doi:10.1007/s00410-015-1194-8.

Schoolmeesters, N., Cheadle, M. J., John, B. E., Reiners, P. W., Gee, J. & Grimes, C. B. (2012). The cooling history and the depth of detachment faulting at the Atlantis Massif oceanic core complex. *Geochemistry, Geophysics, Geosystems* **13**, Q0AG12.

Seher, T., Crawford, W. C., Singh, S. C., Cannat, M., Combier, V. & Dusunur, D. (2010). Crustal velocity structure of the Lucky Strike segment of the Mid-Atlantic Ridge at 37°N from seismic refraction measurements. *Journal of Geophysical Research: Solid Earth* **115**, B03103.

Shaw, A. M., Behn, M. D., Humphris, S. E., Sohn, R. A. & Gregg, P. M. (2010). Deep pooling of low degree melts and volatile fluxes at the 85°E segment of the Gakkel Ridge: Evidence from olivine-hosted melt inclusions and glasses. *Earth and Planetary Science Letters* **289**, 311–322.

Shorttle, O. (2015). Geochemical variability in MORB controlled by concurrent mixing and crystallisation. *Earth and Planetary Science Letters* **424**, doi:10.1016/j.epsl.2015.04.035.

Singh, S. C., Kent, G. M., Collier, J. S., Harding, A. J. & Orcutt, J. A. (1998). Melt to mush variations in crustal magma properties along the ridge crest at the Southern East Pacific Rise. *Nature* **394**, 874–878.

Singh, S. C., Crawford, W. C., Carton, H., Seher, T., Combier, V., Cannat, M., Pablo Canales, J., Dusunur, D., Escartin, J. & Miguel Miranda, J. (2006). Discovery of a magma chamber and faults beneath a Mid-Atlantic Ridge hydrothermal field. *Nature* **442**, 1029–1032.

Sleep, N. H. (1975). Formation of oceanic crust: some thermal constraints. *Journal of Geophysical Research* **80**, 4037–4042.

Solano, J. M. S., Jackson, M. D., Sparks, R. S. J. & Blundy, J. (2014). Evolution of major and trace element composition during melt migration through crystalline mush: Implications for chemical differentiation in the crust. *American Journal of Science* **314**, 895–939.

Suhr, G., Hellebrand, E., Johnson, K. & Brunelli, D. (2008). Stacked gabbro units and intervening mantle: A detailed look at a section of IODP Leg 305, Hole U1309D. *Geochemistry, Geophysics, Geosystems* **9**, doi:10.1029/2008GC002012.

Teagle, D. A. H., Alt, J. C., Umino, S., Miyashita, S., Banerjee, N. R., Wilson, D. S. & Expedition 309/312 Scientists (2006). *Proceedings of the Integrated Ocean Drilling Program, 309/312*. Integrated Ocean Drilling Program Management International, Washington, DC.

Thomas, R. M. (2003). Processes of lower crustal accretion beneath intermediate- to fast-spreading ocean ridges: constraints from the Wadi Abyad section of the Oman ophiolite. PhD thesis, Cardiff University, 497 pp.

Toomey, D. R., Solomon, S. C., Purdy, G. M. & Murray, M. H. (1985). Microearthquakes beneath the median valley of the Mid-Atlantic Ridge near 23°N: Hypocenters and focal mechanisms. *Journal of Geophysical Research* **90**, 5443–5458.

Tormey, D. R., Grove, T. L. & Bryan, W. B. (1987). Experimental petrology of normal MORB near the Kane Fracture Zone: 22°–25°N, mid-Atlantic ridge. *Contributions to Mineralogy and Petrology* **96**, 121–139.

Van Orman, J., Grove, T. & Shimizu, N. (2001). Rare earth element diffusion in diopside: influence of temperature, pressure, and ionic radius, and an elastic model for diffusion in silicates. *Contributions to Mineralogy and Petrology* **141**, 687.

Vera, E. E., Mutter, J. C., Buhl, P., Orcutt, J. A., Harding, A. J., Kappus, M. E., Detrick, R. S. & Brocher, T. M. (1990). The structure of 0 to 0·2 m.y. old oceanic crust at 9°N on the East Pacific Rise from expanded spread profiles. *Journal of Geophysical Research* **95**, 15529–15556.

Villiger, S., Müntener, O. & Ulmer, P. (2007). Crystallization pressures of mid-ocean ridge basalts derived from major element variations of glasses from equilibrium and fractional crystallization experiments. *Journal of Geophysical Research* **112**, B01202.

Wanless, V. D., Perfit, M. R., Ridley, W. I. & Klein, E. (2010). Dacite petrogenesis on mid-ocean ridges: evidence for oceanic crustal melting and assimilation. *Journal of Petrology* **51**, 2377–2410.

Wanless, V. D., Shaw, A. M., Behn, M. D., Soule, S. A., Escartín, J. & Hamelin, C. (2015). Magmatic plumbing at Lucky Strike

volcano based on olivine-hosted melt inclusion compositions. *Geochemistry, Geophysics, Geosystems* **16**, 126–147.

White, W. M. & Bryan, W. B. (1977). Sr-isotope, K, Rb, Cs, Sr, Ba, and rare-earth geochemistry of basalts from the FAMOUS area. *Geological Society of America Bulletin* **88**, 571–576.

Wolfe, C. J., Purdy, G. M., Toomey, D. R. & Solomon, S. C. (1995). Microearthquake characteristics and crustal velocity structure at 29°N on the Mid-Atlantic Ridge: The architecture of a slow spreading segment. *Journal of Geophysical Research* **100**, 24449–24472.

Xu, M., Canales, J. P., Tucholke, B. E. & DuBois, D. L. (2009). Heterogeneous seismic velocity structure of the upper lithosphere at Kane oceanic core complex, Mid-Atlantic Ridge. *Geochemistry, Geophysics, Geosystems* **10**, Q10001.

Xu, M., Pablo Canales, J., Carbotte, S. M., Carton, H., Nedimović, M. R. & Mutter, J. C. (2014). Variations in axial magma lens properties along the East Pacific Rise (9°30′N–10°00′N) from swath 3-D seismic imaging and 1-D waveform inversion. *Journal of Geophysical Research: Solid Earth* **119**, 2721–2744.

Yang, H. J., Kinzler, R. J. & Grove, T. L. (1996). Experiments and models of anhydrous, basaltic olivine–plagioclase–augite saturated melts from 0·001 to 10 kbar. *Contributions to Mineralogy and Petrology* **124**, 1–18.